SLAC-PUB-796
(TH) and (EXP)
September 1970

RECENT RESULTS IN INELASTIC ELECTRON SCATTERING

by

E. D. Bloom, G. Buschhorn*, R. L. Cottrell, D. H. Coward, H. DeStaebler, J. Drees+, C. L. Jordan, G. Miller, L. Mo++, H. Piel and R. E. Taylor†

Stanford Linear Accelerator Center§,
Stanford, California

M. Breidenbach, W. R. Ditzler, J. I. Friedman, G. C. Hartmann**, H. W. Kendall and J. S. Poucher

Physics Department and Laboratory for Nuclear Science§§,
Massachusetts Institute of Technology,
Cambridge, Massachusetts

A Report presented to the XV International Conference on High Energy Physics, Kiev, U.S.S.R.

---

* Present address: DESY, Hamburg, Germany

** Present address: Xerox Corp., Rochester, New York

\+ Present address: Bonn University, Bonn, Germany

++ Present address: Dept. of Physics and the Enrico Fermi Institute, University of Chicago, Chicago, Illinois

† Attending Conference

§ Work supported by the U.S. Atomic Energy Commission

§§ Work supported in part through funds provided by the U.S. Atomic Energy Commission under Contract No. AT(30-1)2098

Introduction

During the past two years, the MIT-SLAC collaboration has performed several experiments on inelastic electron scattering using the spectrometer facility at SLAC. The high energy and the high beam intensity of the linear accelerator at SLAC make possible experiments with good statistical accuracy that extend over a wide range of momentum transfer and recoil missing mass energy. In these experiments only the electron is detected which allows a relatively simple theoretical interpretation in terms of two functions determined by the internal structure of the target particle. For the proton we find that for a wide range of momentum transfer the deep inelastic cross section is approximately proportional to the Mott cross section for point particles, rather than showing the steep dependence on momentum transfer familiar from elastic e-p scattering. The experimental program is continuing, and we have carried out experiments extending the kinematic range of the proton measurements, and recently, have begun measurements on deuterium and other nuclei. Although the analysis of the data from these experiments has not been completed, the interest in the results encourages us to present a status report on the various experiments, together with some results in preliminary form.

We have taken data on the following inelastic scattering experiments since operations began at SLAC in 1967:

1. Inelastic e-p scattering at 6° (1967). The data were reported at the Vienna Conference in 1968.[1]

2. Inelastic e-p scattering at 6° and 10° (1968). This experiment repeated some of the data points presented at Vienna. The data in the deep inelastic have been reported in the literature.[2] Cross sections are available for all data points.[3] Studies of the resonance excitation observed in this experiment are continuing.

3. Inelastic e-p scattering at 1.5° (1968). These measurements were made in order to extract total γp cross sections by extrapolation to $q^2 = 0$.[4] The systematic errors in this experiment are larger than those obtained in direct measurements of photon absorption in bubble chamber and counter experiments. Within the systematic errors, there is agreement between the various experiments. The method of extrapolating electron scattering data has some advantages in the region of resonance excitation. Since the total absorption cross section for photons is a fundamental quantity it is useful to measure it in several ways, particularly when the sources of systematic errors are different.

4. Inelastic e-p scattering at 18°, 26° and 34° (1968). These data were obtained using the 8 GeV spectrometer facility. A preliminary analysis of some of these data has already been reported at various conferences.[5] The final analysis of these data is now almost complete, and some portion of it will be presented in this paper.

5. Inelastic scattering from deuterium (1970). Measurements have been made on hydrogen and deuterium at 6° and 10° with measurements on Be, Cu and Au at 6°. The hydrogen data repeated the older 6° and 10° measurements with somewhat better statistical precision and extended the range of initial energies from 4.5 GeV to 19.5 GeV from roughly 7 GeV to 17 GeV in the older data. The ratio of the deuterium and hydrogen cross sections is obtained at each data point. The analysis of the data is in its early stages, but some very preliminary results are presented. An interesting comparison of data from SLAC and DESY

can be made using data taken in this experiment. The lowest incident energy for the 10° experiment was chosen to be equal to the incident energy of a published DESY spectrum at 10°.[6] In Fig.1 the DESY spectrum is shown, and a few points from the SLAC spectrum are overplotted. The agreement is well within the estimates of systematic errors.

Excitation of Resonances

Resonance excitation is a prominent feature of the data for values of q^2 less than $2.5(\mathrm{GeV}/c)^2$. A recent set of fits to the 1968 data at 6° and 10° is described in an M.I.T. thesis by M. Breidenbach.[3] An example of the fits obtained is shown in Fig.2. The qualitative features of the resonance behavior obtained in these fits are very similar to the results presented at Vienna, but the numerical results for the integrated resonance cross section differ considerably. The changes are the result of different assumptions about the shapes of the individual resonance peaks, and to a lesser extent the form of the background under the peaks. Changes in the form of the resonance tend to change all values of a given resonance cross section by about the same factor, so that a change in resonance shape is largely a matter of normalization. The results of the new fit are shown in Table I. A width of $\sim$ 85 MeV is still preferred for the 1510 resonance, somewhat narrower than the width obtained in π p interactions.

The resonance cross sections for $q^2 \gtrsim 1(\mathrm{GeV}/c)^2$ as shown in Fig. 3 have a q^2-dependence similar to that of the elastic peak. The cross sections for the background under the resonances appear to decrease with q^2 at roughly the same rate as the resonance cross sections. A plot of νW_2 against $2M\nu/q^2$ for the backgrounds extracted in the fitting procedure is shown in Fig. 4, where it is seen that νW_2 roughly follows a single curve. In the recent runs on deuterium we have also taken data in the resonance region. Fig. 5 shows the measured differential cross sections without radiative corrections at $E_o = 7$ GeV, $\theta = 6^\circ$ for hydrogen and deuterium.

Large Angle Data

The MIT-SLAC collaboration has measured e-p inelastic cross sections at 18°, 26°, 34° using the 8GeV spectrometer at SLAC.[7] The experimental method followed closely that used in previous measurements with the 20GeV spectrometer at 6° and 10°.[2] Electrons from the beam analyzing system were scattered from the same hydrogen target used in the forward angle measurements. The scattered electrons were detected in the 8GeV spectrometer. For each angle and each initial energy, the differential cross section $d^2\sigma/d\Omega dE'$ was measured for a range of secondary energies E' from an E' corresponding to elastic scattering to secondary energies of $\sim$ 2GeV.

Pion backgrounds for the lower scattered energies were larger than in the previous work, and a threshold Cerenkov counter was added to the detection system to improve particle discrimination. As in the earlier data, cross sections were measured for a number of incident energies to provide data for the radiative corrections. Values of the cross sections for $W > 1.8$ GeV after radiative corrections are shown in Table II.

In addition to counting statistics the errors quoted in the table include estimates of various other effects which might cause point to point fluctuations in the values of the cross section. Other sources of systematic error are being studied and have not been included in the estimates of error in the table. The systematic errors are expected to be less than 5% for the points in the table.

Structure Functions of the Proton

The data, together with the data from 6° and 10°, can be used to evaluate separately the structure functions W_1 and W_2 (or σ_T and σ_S) over a large region of four momentum transfer squared, q^2, and energy loss, ν. In the one photon approximation, Fig.6, the differential cross section can be written

$$\frac{d^2\sigma}{d\Omega dE'} = \sigma_{NS}\left[W_2(q^2,\nu) + 2\ tg^2\ \theta/2\ W_1(q^2,\nu)\right]$$

or, equivalently,

$$\frac{d^2\sigma}{d\Omega dE'} = \Gamma_t\left[\sigma_T(q^2,W) + \epsilon\,\sigma_S(q^2,W)\right]$$

where

$$q^2 = -(p - p')^2 = 4EE'\sin^2\theta/2$$

$$\nu = \frac{P\cdot q}{M} = E - E'$$

The invariant missing mass, W, can be expressed as

$$W^2 = (P + q)^2 = M^2 - q^2 + 2M\nu = s$$

M = mass of the proton

$$\sigma_{NS} = \frac{4\alpha^2 E'^2 \cos^2 \theta/2}{q^4}$$

$$\Gamma_t = \frac{\alpha}{2\pi^2} \frac{K}{q^2} \frac{E'}{E} \frac{1}{1-\epsilon}, \qquad K = \frac{W^2 - M^2}{2M}$$

$$\epsilon = \frac{1}{1 + 2(1 + \nu^2/q^2) \, tg^2 \, \theta/2}$$

The two descriptions of the cross section are equivalent

and

$$W_1 = \frac{K}{4\pi^2 \alpha} \sigma_T$$

$$W_2 = \frac{K}{4\pi^2 \alpha} \frac{q^2}{(q^2+\nu^2)} (\sigma_T + \sigma_S)$$

By making measurements at several angles for given values of q^2 and ν, values of W_1 and W_2 (or σ_T and σ_S) can be determined. The separation can be expressed as a value for one of the two structure functions and the ratio $R = \sigma_S / \sigma_T$. The experiments were programmed so that at several angles there are data points at $q^2 = 4(\text{GeV/c})^2$, W = 2, 3, 4 GeV. At these points the separation is straightforward, (Fig.7). At other points interpolation of the data is required to provide cross sections for the separation. Data for constant incident energy, constant scattering angle, and varying secondary energy lie along a straight line in the q^2, ν plane. Fig. 8 shows the lines on which we have data in the q^2 - ν plane. In the shaded region of Fig. 8 separations of the structure functions have been made using several

different methods of interpolation. The values of R obtained are not very sensitive to the method of interpolation. Values of R and the structure functions at twenty-three different values of ν and q^2 are shown in Table III. The errors shown in the table are obtained from a fit to interpolated cross sections and do not include all possible systematic errors in the data or systematic errors arising in the interpolation procedure. Such errors are expected to be smaller than the quoted errors. From these measured values it is clear that the ratio $R = \sigma_S / \sigma_T$ is small compared to one. R exhibits no striking variations with the kinematic variables. A constant value for R is consistent with our data, and a value of $R = 0.18 \pm .05$ is obtained by averaging the values in the table. Systematic errors may be quite important compared to the error for the average R. It is quite unlikely, but not impossible, that the interaction is purely transverse ($R = 0$). This conclusion may be altered after studying the possible sources of error more thoroughly. The values of R obtained are also compatible with $R = a\, q^2$, with $a \approx 0.035 (\mathrm{GeV}/c)^{-2}$, and with $R = q^2/\nu^2$. These two forms are suggested by theoretical considerations. Undoubtedly, various other forms are also compatible with our results.

Fig. 9 shows the values of σ_T obtained in the separations at $W = 2$ GeV and $W = 3$ GeV, as a function of q^2. The q^2 dependence of the ρ propagator(squared) is shown for comparison. Fig. 10 shows the values of $2MW_1$ and νW_2 obtained in the separation plotted against the variable $\omega = 2M\nu / q^2$. Bjorken[8] has conjectured that, in the limit as $q^2 \to \infty$ with the ratio ν/q^2 fixed, the structure functions W_1 and νW_2 would be functions of ν/q^2 only. This property has become known as "scaling." For $q^2 \gtrsim 1 (\mathrm{GeV}/c)^2$ and $W \geq 2$ GeV, values of νW_2 and W_1 from the 6° and 10° data could be described (within errors) by single functions of ν/q^2,

if the ratio R was assumed to be zero.[2] If we now assume some functional form for R over the full range of the data, compatible with the measurements of R, values of W_1 and νW_2 (or σ_S and σ_T) can be obtained for all the data points. These structure functions can then be tested for consistency with scaling in the variable $\omega \equiv 2M\nu/q^2$ for the finite values of q^2 in our experiment.

Assuming a constant value R = 0.18, values of $2MW_1$ and νW_2 are plotted in Figs. 11 and 12 with $q^2 \gtrsim 1(\text{GeV}/c)^2$, $W \gtrsim 2$ GeV. It is evident that the structure functions exhibit at least roughly the conjectured scaling behavior. Taking $R = q^2/\nu^2$ or $R = 0.035\ q^2$ does not change the behavior of W_1 or νW_2 appreciably, although for $R = 0.035\ q^2$ the variations with q^2 near $\omega = 1$ are a little smaller.

The relationship between W_1 and W_2 is such that if $R = q^2/\nu^2$, then

$$2MW_1 = 2M\nu/q^2 \cdot \nu W_2$$

and, therefore, $2MW_1$ "scales" automatically if νW_2 scales. The relationship $R = q^2/\nu^2$ follows if the matrix elements for transverse and longitudinal electromagnetic currents are equal.

To examine the behavior of νW_2 for $W \gtrsim 2$ GeV, $q^2 \gtrsim 1(\text{GeV}/c)^2$ under the assumption $R = 0.18$ in more detail, it is convenient to consider three regions of ω.

I. ω in the range $3.5 < \omega < 10$

In this region the data exhibit scaling behavior within errors for $W \gtrsim 2$ GeV, $q^2 \gtrsim 1(\text{GeV}/c)^2$. The data cover more than a decade of variation in q^2 and in ν. Fig. 13 shows νW_2 at $\omega = 2M\nu/q^2 = 4$, as a function of q^2 for $W \gtrsim 2$ GeV. The goodness of

fit of the data in Fig. 13 to a constant is a measure of the goodness of "scaling." In the region $3.5 < \omega < 10$ data for all ω are consistent with a single value of νW_2.

II. ω in the range $1 < \omega < 3.5$

In this region the restrictions $W > 2$ GeV, $q^2 \geq 1$ GeV eliminate much of the data from forward angles and reduce the range of q^2 at a given value of ω. While a fit to a single function for νW_2 can be made for $W \geq 2.2$ GeV, for ω near 1 deviations from scaling behavior are evident in Fig. 12, with νW_2 decreasing with increasing q^2. Observing that νW_2 is constrained to zero at threshold, we attempted to fit νW_2 with expressions of the form

$$\nu W_2 = \sum_{n = n_1}^{n_2} a_n \quad (1 - 1/\omega)^n = \sum \frac{a_n}{(1 + q^2/(W^2 - M^2))^n}$$

A satisfactory fit was achieved for $n_1 = 3$ and $n_2 = 5$. The leading term is suggestive of the result of Drell and Yan[9] that there should be a connection between νW_2 threshold behavior and the elastic form factor. Note that for $n = 3$

$$W_2 \alpha \frac{1}{(1 + q^2/(W^2 - M^2))^4}$$

which is similar to the dipole approximation to the elastic form factors

$$G^2 = \frac{1}{(1 + q^2/.71)^4}$$

except that this expression for W_2 is exactly zero at the elastic peak, $W^2 = M^2$. In order to avoid this feature at $W^2 = M^2$ we also fitted with a similar expression but introducing an additional adjustable constant, replacing $(1 - 1/\omega)$ by

$$(1 - 1/\omega') = \left[1 + \frac{q^2}{W^2 - M^2 + a}\right]^{-1} \quad , a > 0$$

A fit gives $a \sim .9(\mathrm{GeV}/c)^2$, and with this value the data can be fitted satisfactorily for $W > 1.8$ GeV. With this change the expression for νW_2 is no longer constrained to zero at the elastic peak. Fig. 14 shows a νW_2 plot at $\omega = 1.66$ for different values of q^2. The solid curve is the fit using ω', which is seen to fit the data points better than a horizontal line which would indicate scaling with ω. Another way to see the improvement is illustrated in Fig. 15, where values of νW_2 are plotted against ω'. The points near $\omega' = 1$ clearly cluster more closely than in Fig. 12.

The variable ω' is related to ω by

$$\omega' = \omega + a/q^2$$

so that in the Bjorken limit $\omega' = \omega$. For the particular value, $a = 0.88\ \mathrm{GeV}^2 = M^2$

$$\omega' = 1 + s/q^2 \qquad (s = W^2)$$

In the kinematic region covered by our measurements where q^2 and

ν may not be "large" in the sense of the Bjorken limit, it is worth emphasizing the possibility that some variable other than ω (but approaching ω in the limit) may have physical significance. Bloom and Gilman[10] have speculated about some consequences suggested by the ω' fit.

III. ω in the range $\omega > 10$

The data in this region are rather sparse, and we emphasize that q^2 for most of the points is not far from $1(\mathrm{GeV}/c)^2$, and that large ω tends to be correlated with low q^2. While νW_2 appears to decrease for increasing ω (assuming $R = 0.18$), the decrease is not demonstrated convincingly. The data taken in 1970 allow a more detailed study of this region, and a discussion based on a preliminary analysis of the data is included in the next section.

New Data on e-p Inelastic Scattering

In the most recent experiment performed by the MIT-SLAC group, data for both hydrogen and deuterium have been obtained. The experimental method and the analysis of the hydrogen data follow closely the procedures used for the older data at 6° and 10°. A threshold Cerenkov counter was added to the detector array of the 20-GeV spectrometer to improve π-e separations. Preliminary results from the first analysis of the proton data agree within errors with the results of the older 6° and 10° data where the measurements overlap. In the most recent experiment, measurements were made at an initial energy of 19.5 GeV, increasing the values of q^2 available at a given ω. The recent measurements have increased statistical accuracy, and, in the deep inelastic region, the density of points in E' is approximately

double that of the older data. At the present stage of the analysis possible systematic errors have not been fully investigated, errors comparable to those quoted for the older data (5% for E' greater than 5 GeV, increasing to 10% at E' $\approx$2 GeV) should be assigned to the data.

The new data extend considerably the information available for $\omega \gtrsim 10$. It should be emphasized that in this region we have no experimental information on the value of R, and that the value of νW_2 is more sensitive to R for the higher values of ω. There are two questions which we would like to answer in the region $\omega > 10$. First, do the results exhibit scaling behavior, and if so, are the values of νW_2 in this region equal to the value of νW_2 for $3.5 < \omega < 10$? Assuming $R = 0.18$, Fig. 16 shows the behavior of the data for $\omega > 10$, $q^2 > 0.5(\mathrm{GeV/c})^2$. The data all lie within $\pm$ 20 % of an average curve, but variation is evident as q^2 decreases below $\sim 1(\mathrm{GeV/c})^2$. The variation appears to be a decrease of νW_2 with decreasing q^2. Such a variation is also observed for $q^2 < 1(\mathrm{GeV/c})^2$ in the data with $3.5 < \omega < 10$. Note that for $q^2 = 0$, $\nu W_2 = 0$, so that there must be a region in q^2 where νW_2 does not scale. In Fig. 17 we have plotted νW_2 against q^2 for several different ranges of ω. For the lower values of ω, νW_2 is seen to increase with q^2 up to about $q^2 \sim 1(\mathrm{GeV/c})^2$ and apparently levels off above this value of q^2, becoming constant within errors. The behavior at high ω is not inconsistent with this same kind of behavior, but the data can not exclude a different behavior. If we assume that at the high values of ω, νW_2 is constant above $q^2 = 1(\mathrm{GeV/c})^2$ and fit a constant to the data for each value of ω, then we find that νW_2 does decrease significantly above $\omega = 10$ as shown in Fig. 18. A similar analysis for each of the two other assumptions for R, $R = 0.035\ q^2$, and $R = q^2/\nu^2$, show even stronger decreases, but we wish to emphasize again the lack of experimental information for R in this region of ω.

In summary, we are unable to demonstrate scaling behavior for νW_2 at large values of ω, although the data are not inconsistent with such behavior. Assuming scaling behavior, and 'reasonable' values for R in this region of ω, νW_2 appears to decrease as ω increases.

Inelastic Electron Scattering from Deuterium

The analysis of the deuterium data recently taken at 6° and 10° has only just begun. The radiative corrections to the deuteron data are somewhat more complex than for hydrogen. We have made some initial studies of the radiative corrections and of the effects of "smearing" arising from the internal motion of the proton and neutron in the deuteron. We are presenting some data from this preliminary analysis in which the application of preliminary radiative corrections does not change the value of the cross section ratio D/H by more than 3% compared to the ratio before any radiative corrections are made. The values given in Table IV include the preliminary radiative corrections. The errors are obtained by adding 3% to the statistical errors for the corrected deuterium cross section and then adding this modified error in quadrature with the statistical errors of the hydrogen data. The resulting errors are no longer wholly random but contain a certain component of estimated systematic errors.

In Fig. 19 we have plotted values of the ratio D/H against q^2 for four values of W. Points for $q^2 = 0$ have been taken from experiments on total photon absorption.[11] The ratio is seen to decrease markedly with increasing q^2 for low values of W.

Corrections for internal motion, final state interactions and Glauber corrections have not been made but are believed to be small in the kinematic

ranges of the measurements presented. Therefore, the deuterium scattering can be taken to a good approximation, equal to the sum of proton and neutron scattering. In what follows, neutron cross sections mean (D/H-1) multiplied by the appropriate proton cross section.

Neutron cross sections appear to become significantly smaller than the corresponding proton cross sections as q^2 increases. If we assume that R for the neutron equals R for the proton , i.e.,the transverse photon interactions dominate the neutron scattering as they do the proton scattering for these kinematics, we can roughly test whether or not the neutron structure functions exhibit scaling. Values of (D/H - 1) plotted against ω are shown in Fig. 20 . The values of the ratio are consistent with a single function of ω and so within the rather large errors the neutron exhibits scaling.

Preliminary values of some integrals related to various energy weighted sum rules[12-14] can be estimated by integrating the proton data and the preliminary neutron data under the assumption that $R_{proton} = R_{neutron} = 0.18$. The upper limit of the integrals, $\omega = 12$, corresponds to the largest ω for which the neutron data have been analyzed. For the proton we find

$$I_{1p} = \int_1^{12} \frac{d\omega}{\omega^2} (\nu W_{2p}) = 0.14, \quad I_{2p} = \int_1^{12} \frac{d\omega}{\omega} (\nu W_{2p}) = 0.58$$

and for the neutron

$$I_{1n} = \int_1^{12} \frac{d\omega}{\omega^2} (\nu W_{2n}) = 0.10 , \quad I_{2n} = \int_1^{12} \frac{d\omega}{\omega} (\nu W_{2n}) = 0.45$$

Error estimates including the possibility that νW_2 scales in ω' rather than ω give $\pm$ 15% for I_{1p} and I_{1n} and $\pm$ 10% for I_{2p} and I_{2n}. In addition a change of $\pm$ 0.1 in R introduces a change of $\pm$ 4% in the integrals.

The difference between I_{2p} and I_{2n},[15]

$$\int_1^{12} \frac{d\omega}{\omega} \left[(\nu W_{2p}) - (\nu W_{2n}) \right] = 0.13$$

and has an uncertainty which is dominated by systematic effects. We estimate this uncertainty will not be more than 40%. Inspection of Fig. 20 indicates that the neutron-proton cross section ratio is less than unity over much of this range of ω, and hence that the difference $(I_{2p} - I_{2n})$ is greater than zero.

To estimate $(I_{2p} - I_{2n})$ for $\omega_{max} = \infty$ it is necessary to assume a functional behavior for $\nu W_{2p} - \nu W_{2n}$. If we take

$$\nu W_{2p} - \nu W_{2n} = .03 \left(\frac{12}{\omega}\right)^{\alpha} , \quad 12 \leqslant \omega \leqslant \infty$$

which approximately equals the observed difference near $\omega = 12$, and where $\alpha > 0$ is an arbitrary constant, then

$$\int_1^{\infty} \frac{d\omega}{\omega} \left[(\nu W_{2p}) - (\nu W_{2n}) \right] = 0.13 + \frac{.03}{\alpha}$$

The constant q^2 sum rule inequality[15]

$$\int_1^\infty \frac{d\omega}{\omega} \left[\nu W_{2p} + \nu W_{2n} \right] \geq \frac{1}{2}$$

appears to be satisfied for $\omega \gtrsim 5$.

While much of the data presented are still preliminary and should therefore be treated with some caution, it does appear that the neutron structure function W_{2n} is quite different than that of the proton over much of the range of our data. This indicates that the scattering from the nucleon includes a non-diffractive component which is different for the neutron and the proton. The results for $\nu W_{2p} - \nu W_{2n}$ shown in Fig. 21a suggest a possible bump with a tail toward increasing ω. Scaling and a peak in $\nu W_{2p} - \nu W_{2n}$ follow naturally from certain theoretical models involving quasi-free point-like constituents. Some examples of these models are shown in Fig. 21b.

REFERENCES

1. W. K. H. Panofsky in Proceedings of the Fourteenth International Conference on High-Energy Physics, Vienna, Austria, September, 1968, (CERN Scientific Information Service, Geneva, Switzerland, 1969).

2. E. D. Bloom, D.H. Coward, H. DeStaebler, J. Drees, G. Miller, L.W. Mo, R. E. Taylor, M. Breidenbach, G.C. Hartmann, and H. W. Kendall, Phys. Rev. Letters 23, 930 (1969); M. Breidenbach, J. I. Friedman, H. W. Kendall, E. D. Bloom, D. H. Coward, H. DeStaebler, J. Drees, L.W. Mo, and R. E. Taylor, Phys. Rev. Letters 23, 935 (1969).

3. M. Breidenbach, "Inelastic Electron-Proton Scattering at High Momentum Transfer," Dissertation, Massachusetts Institute of Technology, Cambridge, Massachusetts, May, 1970. MIT Report No. 2098-635. This thesis contains a sampling of the data. Complete sets of cross sections are available from the authors at MIT or at SLAC.

4. E. D. Bloom, R. L. Cottrell, D. H. Coward, H. DeStaebler, J. Drees, G. Miller, L.W. Mo, R. E. Taylor, J. I. Friedman, G. C. Hartmann, and H. W. Kendall, SLAC-PUB-653, Stanford Linear Accelerator Center, Stanford, California, September, 1969 (unpublished).

5. R. E. Taylor in Fourth International Symposium on Electron and Photon Interactions at High Energies, 1969, (Daresbury Nuclear Physics Laboratory, Keckwick Lane, Daresbury, Nr. Warrington, Lancashire, England, 1969), and in Conference on Expectations for Particle Reactions at the New Accelerators, March, 1970, (University of Wisconsin, Madison, Wisconsin, 1970).

6. W. Bartel, B. Dudelzak, H. Krehbiel, J. McElroy, U. Meyer-Berkhout, W. Schmidt, V. Walther and G. Weber, Phys. Letters 28B, 148 (1968).

7. R. E. Taylor in Proceedings of the 1967 International Symposium on Electron and Photon Interactions at High Energies, (Stanford Linear Accelerator Center, Stanford, Calif., 1967).

8. J. D. Bjorken, Phys. Rev. 179, 1547 (1969).

9. S. D. Drell and T-M. Yan, Phys. Rev. Letters 24, 181 (1970).

10. E. D. Bloom and F.J. Gilman, SLAC-PUB-779, Stanford Linear Accelerator Center, Stanford, Calif., June, 1970. (Submitted to Phys. Rev. Letters).

11. D. O. Caldwell, V.B. Elings, W.B. Hesse, R.J. Morrison, F.V. Murphy, B.W. Worster, and D.E. Yount, Preprint, University of California, Santa Barbara, Calif., April, 1970. (Unpublished).
H. Meyer, B. Noroska, J.H. Weber, M. Wong, V. Heynen, E. Mandelkow, and D. Notz, Preprint, Deutsches Elektronen-Synchrotronen, DESY, Hamburg, Germany, May, 1970. (Unpublished).

12. J. D. Bjorken and E. A. Paschos, Phys. Rev. 185, 1975-82 (1969).

13. C. G. Callan, Jr. and D. J. Gross, Phys. Rev. Letters 21, 311 (1968).

14. K. Gottfried, Phys. Rev. Letters 18, 1174 (1967).

15. J. D. Bjorken, in Selected Topics in Particle Physics, Proceedings of the International School of Physics "Enrico Fermi", Course XLI, Edited by J. Steinberger (Academic Press, Inc., New York, 1968).

TABLE CAPTIONS

Table I. Parameters of the resonances and resonant cross sections for 1968 6° and 10° data. The errors given in the table are statistical errors arising from the fit and do not include systematic errors in the data or the uncertainties arising from the assumptions made for resonance shapes and the form of the background. A detailed discussion of the data and fitting procedures can be found in Ref. 2.

Table II. Cross sections for $W \geq 1.8$ GeV for e-p scattering at 18°, 26° and 34°. The tables do not include systematic errors, estimated to be less than 5%.

Table III. Values of the structure functions and $R = \sigma_S / \sigma_T$ from 6°, 10°, 18°, 26°, 34° data. Three of the values at $q^2 = 4(\text{GeV}/c)^2$, $W = 2$, 3, 4 GeV are taken directly from measured cross sections. The twenty remaining points involve some interpolation of data.

Table IV. Preliminary values of the ratios of the deuterium and hydrogen cross sections.

TABLE 1a

Resonance Parameters Obtained in the Fitting Procedures		
	Mass (GeV)	Width (GeV)
First	1.226 ± .005	0.115 ± .010
Second	1.508 ± .005	0.080 ± .020
Third	1.705 ± .015	0.085 ± .025

The mass and width of the fourth resonance were fixed during the fitting procedure, at a mass of 1.92 GeV and a width of 0.22 GeV.

TABLE 1b

		First	Second	Third	Fourth
Resonance Amplitudes Obtained in the Fitting Procedure given in Units of 10^4 pb/GeV-sr					
6^o	7.0	690. ± 20.	223. ± 10.	160. ± 10.	49. ± 5.
	10.0	132. ± 10.	68. ± 5.	55. ± 5.	11. ± 3.
	13.5	19. ± 2.	17. ± 2.	15. ± 2.	1.1 ± 1.
	16.0	5.2 ± .7	7.2 ± .7	6.4 ± .6	1.3 ± .6
10^o	7.0	20. ± 1.	14. ± 1.	11. ± 2.	2.3 ± 1.
	11.0	0.81 ± .12	1.4 ± .2	1. ± .4	0.16 ± .3
	13.5	< 0.15	< 0.63	< 0.8	
	15.2	< .09	< 0.25	< 0.22	
	17.7	< .035	< .07	< .075	

TABLE 1c

	First	Second	Third	Fourth
Resonance Cross Sections for 6^o Data in Units of 10^5 pb/sr				
7.0	11. ± 1.	5.3 ± .9	4.6 ± .7	2.6 ± .5
10.0	2.2 ± .2	1.3 ± .2	1.0 ± .2	0.55 ± .18
13.5	0.37 ± .03	0.25 ± .03	0.27 ± .04	.063 ± .08
16.0	.095 ± .009	.094 ± .015	0.12 ± .03	.066 ± .03
Resonance Cross Sections for 10^o Data in Units of 10^3 pb/sr				
7.0	34. ± 2.	21. ± 3.	25. ± 5.	15. ± 5.
11.0	1.1 ± .3	1.6 ± .4	1.5 ± .7	0.73 ± 1.5
13.5	< .35	< .7	< 1.3	
15.2	< .13	< .28	< .58	
17.7	< .06	< .08	< .12	

Note: The errors in the tables reflect the statistical uncertainties of the fits but do not include any estimate of the errors due to the assumed shapes for the resonances and background.

TABLE II

Radiatively Corrected Cross Sections for $W \geq 1.8$ GeV

θ (deg)	E (GeV)	E' (GeV)	$d^2\sigma/d\Omega dE'$ (10^{-35} cm^2/sr-GeV)
18	4.501	2.250	7600. ± 430.
		2.000	7000. ± 450.
	6.503	3.500	1879. ± 54.
		3.000	2413. ± 75.
		2.500	2593. ± 93.
		2.000	2510. ± 120.
	8.598	4.780	460. ± 15.
		4.500	572. ± 17.
		4.000	779. ± 44.
		3.500	957. ± 36.
		3.000	1036. ± 50.
		2.500	1229. ± 65.
		2.000	1330. ± 130.
	10.404	5.500	180.6 ± 6.3
		5.000	284. ± 10.
		4.500	409. ± 16.
		3.940	512. ± 23.
		3.500	604. ± 32.
		3.000	630. ± 40.
		2.500	751. ± 47.
		2.000	801. ± 99.
	13.299	7.000	19.88 ± .90
		6.500	49.2 ± 1.9
		6.000	93.0 ± 3.6
		5.500	135.8 ± 5.6
		5.000	178.2 ± 7.7
		4.500	208. ± 15.
		4.000	263. ± 21.
		3.500	306. ± 28.
		3.090	315. ± 23.
		2.500	417. ± 49.
		2.000	533. ± 74.
	17.000	8.000	7.08 ± .35
		7.500	15.17 ± .56
		7.000	29.9 ± 1.1
		6.500	44.8 ± 1.7
		6.000	64.3 ± 2.6
		5.500	86.9 ± 3.4
		5.000	101.1 ± 7.4
		4.500	122.8 ± 9.4
		4.000	145. ± 12.
		3.500	173. ± 16.
		3.000	191. ± 20.
		2.500	239. ± 31.
		2.000	271. ± 54.
26	4.494	2.000	1410. ± 67.
		1.800	1518. ± 81.
26	6.700	2.940	212.6 ± 7.8
		2.750	283.1 ± 10.
		2.500	340. ± 14.
		2.250	407. ± 19.
		2.000	504. ± 25.
		1.750	585. ± 51.
	8.696	3.750	32.2 ± 2.0
		3.500	57.2 ± 3.0
		3.250	91.7 ± 3.7
		3.000	119.9 ± 5.0
		2.750	154.9 ± 6.8
		2.500	195.5 ± 9.7
		2.270	229. ± 12.
		2.000	275. ± 17.
		1.750	317. ± 20.
	11.905	4.500	4.70 ± .48
		4.250	9.34 ± .99
		4.000	17.7 ± 1.0
		3.750	25.9 ± 1.6
		3.500	35.1 ± 2.2
		3.250	47.0 ± 4.5
		3.000	63.4 ± 5.2
		2.750	76.9 ± 7.7
		2.500	91.2 ± 9.9
		2.250	113. ± 12.
		2.000	121. ± 17.
		1.670	161. ± 23.
	15.006	5.000	1.34 ± .17
		4.750	2.87 ± .26
		4.500	5.55 ± .39
		4.250	8.07 ± .50
		4.000	13.83 ± .91
		3.750	18.4 ± 1.5
		3.500	23.3 ± 1.3
		3.250	31.6 ± 1.8
		3.000	39.6 ± 2.3
		2.750	45.9 ± 4.3
		2.500	52.0 ± 5.4
		2.250	62.7 ± 7.6
		2.000	76. ± 10.
		1.750	79. ± 15.
	18.030	5.500	.500 ± .090
		5.250	1.09 ± .15
		5.000	1.31 ± .20
		4.750	2.76 ± .29
		4.500	4.78 ± .39
		4.250	7.66 ± .55
		4.000	10.14 ± .99
26	18.030	3.750	12.9 ± 1.2
		3.500	15.3 ± 1.7
		3.250	21.5 ± 1.7
		3.000	25.7 ± 2.5
		2.750	32.9 ± 4.1
		2.500	39.4 ± 5.2
		2.250	45.7 ± 7.3
		2.000	56. ± 10.
		1.750	81. ± 16.
34	4.501	1.600	404. ± 22.
		1.400	533. ± 31.
		1.200	652. ± 41.
	5.795	2.020	108.0 ± 7.6
		1.750	175.3 ± 9.6
		1.500	252. ± 21.
		1.250	356. ± 33.
	7.899	2.500	24.8 ± 1.6
		2.250	38.2 ± 3.3
		2.000	62.4 ± 5.1
		1.750	90.4 ± 8.0
		1.480	125. ± 12.
		1.250	153. ± 21.
	9.999	3.000	3.02 ± .35
		2.750	8.60 ± .57
		2.500	15.03 ± .86
		2.250	26.1 ± 1.2
		2.000	36.4 ± 2.9
		1.750	47.2 ± 4.4
		1.500	70.3 ± 7.4
		1.250	104. ± 13.
	12.500	3.250	1.22 ± .19
		3.000	3.52 ± .40
		2.750	7.57 ± .55
		2.500	10.32 ± .64
		2.250	17.1 ± 1.7
		2.000	21.9 ± 2.4
		1.750	32.1 ± 4.0
		1.500	47.8 ± 6.6
		1.250	61. ± 13.
	14.996	3.250	0.85 ± .25
		3.000	2.29 ± .38
		2.750	4.30 ± .53
		2.500	7.21 ± .99
		2.250	11.8 ± 1.8
		2.000	16.7 ± 2.0
		1.750	19.6 ± 3.0
		1.500	32.6 ± 5.4

TABLE III

q^2 $(GeV/c)^2$	W GeV	σ_T 10^{-30} cm^2	σ_S 10^{-30} cm^2	R	$2M_pW_1$	νW_2
1.5	2.0	42.8 ± 5.3	-2.8 ± 6.6	-.06 ± .15	1.19 ± .15	.290 ± .012
1.5	2.5	31.7 ± 3.3	4.8 ± 3.7	.15 ± .13	1.52 ± .16	.344 ± .005
1.5	3.0	26.7 ± 2.8	5.4 ± 3.3	.20 ± .14	1.93 ± .20	.343 ± .007
1.5	3.3	25.3 ± 2.8	5.8 ± 3.6	.23 ± .17	2.26 ± .25	.347 ± .011
3.0	2.0	16.1 ± 1.9	.75 ± 2.6	.05 ± .17	.45 ± .05	.179 ± .009
3.0	2.5	15.8 ± 1.5	2.0 ± 2.0	.12 ± .14	.76 ± .07	.265 ± .008
3.0	3.0	15.7 ± 1.6	1.7 ± 2.2	.11 ± .15	1.14 ± .11	.314 ± .014
3.0	3.4	13.3 ± 2.0	4.3 ± 2.8	.32 ± .26	1.27 ± .19	.349 ± .019
4.0	2.0	8.8 ± 1.3	2.0 ± 1.7	.23 ± .23	.244 ± .038	.131 ± .005
4.0	3.0	11.0 ± 1.7	2.0 ± 1.2	.18 ± .18	.799 ± .086	.284 ± .016
4.0	4.0	9.0 ± 1.7	4.5 ± 3.0	.50 ± .43	1.22 ± .23	.369 ± .039
5.0	2.0	5.82 ± .63	1.0 ± .9	.17 ± .17	.162 ± .018	.092 ± .004
5.0	2.5	7.38 ± .57	1.1 ± .8	.15 ± .12	.353 ± .027	.169 ± .005
5.0	3.0	8.23 ± .65	1.4 ± 1.0	.17 ± .13	.596 ± .047	.240 ± .009
5.0	3.4	8.0 ± 1.2	2.2 ± 1.8	.27 ± .27	.763 ± .113	.289 ± .019
8.0	2.0	1.82 ± .25	.58 ± .35	.32 ± .24	.051 ± .007	.039 ± .002
8.0	2.5	2.95 ± .27	.57 ± .41	.20 ± .16	.141 ± .013	.087 ± .004
8.0	3.0	3.55 ± .33	1.30 ± .59	.37 ± .20	.257 ± .024	.157 ± .009
8.0	3.5	4.15 ± .54	1.6 ± 1.1	.39 ± .30	.420 ± .055	.224 ± .021
8.0	4.0	4.99 ± .74	.3 ± 1.8	.06 ± .37	.67 ± .10	.235 ± .048
11.0	2.0	.74 ± .16	.34 ± .23	.46 ± .40	.021 ± .004	.020 ± .001
11.0	2.5	1.44 ± .18	.28 ± .28	.20 ± .22	.069 ± .008	.048 ± .003
11.0	3.0	1.82 ± .22	.89 ± .41	.49 ± .29	.132 ± .016	.102 ± .008

θ (deg)	E (GeV)	E' (GeV)	q^2 $(GeV/c)^2$	W (GeV)	D/H
5.988	10.03	6.760	0.739	2.504	1.87 ± .16
		6.095	0.667	2.755	1.82 ± .15
		5.367	0.587	3.006	1.86 ± .16
		4.577	0.501	3.256	1.93 ± .18
	13.54	9.863	1.457	2.515	1.81 ± .14
		9.230	1.364	2.758	1.79 ± .14
		8.514	1.258	3.010	1.97 ± .17
		7.743	1.144	3.259	1.85 ± .15
		6.916	1.022	3.506	1.98 ± .16
		6.008	0.887	3.759	1.83 ± .14
	16.06	12.05	2.110	2.512	1.67 ± .10
		11.40	1.997	2.762	1.77 ± .12
		10.69	1.873	3.014	1.88 ± .15
		9.951	1.743	3.256	1.95 ± .16
		9.113	1.597	3.510	1.89 ± .15
		8.243	1.444	3.756	1.90 ± .17
		7.277	1.275	4.011	1.84 ± .17
	19.54	14.94	3.184	2.516	1.61 ± .11
		14.32	3.053	2.760	1.69 ± .12
		13.63	2.905	3.011	1.72 ± .13
		12.86	2.741	3.267	1.79 ± .14
		12.05	2.568	3.516	1.75 ± .14
5.988	19.54	11.20	2.388	3.759	1.84 ± .16
		10.28	2.191	4.008	1.78 ± .14
10.000	7.02	4.286	0.913	2.256	1.80 ± .15
		3.716	0.792	2.506	1.86 ± .16
	11.00	7.420	2.478	2.261	1.71 ± .13
		6.887	2.300	2.508	1.68 ± .13
		6.284	2.098	2.761	1.72 ± .14
		5.646	1.886	3.005	1.85 ± .15
		4.942	1.650	3.254	1.78 ± .16
	13.54	9.260	3.807	2.258	1.62 ± .12
		8.742	3.594	2.507	1.61 ± .12
		8.163	3.356	2.758	1.61 ± .13
		7.545	3.102	3.003	1.74 ± .14
		6.847	2.815	3.259	1.79 ± .15
		6.109	2.512	3.508	1.85 ± .17
		5.331	2.192	3.753	1.90 ± .17
		4.473	1.839	4.006	1.90 ± .18
	15.19	10.79	4.98	2.042	1.45 ± .11
		10.37	4.79	2.266	1.54 ± .11
		9.87	4.55	2.515	1.54 ± .12
		9.32	4.30	2.758	1.69 ± .14
		8.71	4.02	3.006	1.69 ± .13
10.000	15.19	8.027	3.704	3.260	1.71 ± .15
		7.304	3.371	3.509	1.82 ± .16
		6.538	3.017	3.756	1.70 ± .15
		5.706	2.633	4.006	1.86 ± .18
	17.69	11.99	6.44	2.263	1.48 ± .12
		11.50	6.18	2.513	1.56 ± .13
		10.95	5.88	2.764	1.52 ± .12
		10.37	5.57	3.005	1.68 ± .14
		9.714	5.22	3.259	1.75 ± .14
		9.028	4.85	3.504	1.79 ± .15
		8.259	4.44	3.760	1.78 ± .16
		7.463	4.01	4.007	1.83 ± .17
	19.33	13.01	7.64	2.260	1.47 ± .11
		12.52	7.35	2.510	1.49 ± .11
		11.99	7.04	2.758	1.51 ± .11
		11.40	7.00	3.009	1.57 ± .12
		10.79	6.33	3.252	1.61 ± .13
		10.08	5.92	3.509	1.64 ± .13
		9.345	5.49	3.758	1.69 ± .14
		8.581	5.04	4.001	1.72 ± .15

TABLE IV

FIGURE CAPTIONS

Fig. 1 Comparison of measured inelastic e-p scattering cross sections from DESY and SLAC at $E_o = 4.879$ GeV, $\theta = 10^o$. The hydrogen target thicknesses are comparable. Only a sample of the SLAC data, heavy points, is shown.

Fig. 2 Resolution of the 10 GeV, 6^o, electron spectrum into four modified Breit-Wigner shapes and a smoothly varying background. Details can be found in Ref. 2.

Fig. 3 q^2 dependence of the resonance cross sections integrated over E' and divided by the elastic scattering cross section. (Ref. 2.)

Fig. 4 νW_2 in the resonance region after the fitted resonances have been subtracted. In this figure νW_2 is derived from the smoothly varying background contribution to the spectrum (see Fig. 2, for example). R = 0.2 was assumed. The errors are statistical errors from the fits. See Ref. 2.

Fig. 5 Electron scattering cross sections for a) hydrogen and b) deuterium in the region of resonance excitation. The elastic peak, and the radiative tails corresponding to elastic scattering have been subtracted.

Fig. 6 Kinematics of inelastic electron-nucleon scattering. p and p' are the four-momentum of the incident electron and final electron, q, is that of the exchanged virtual photon, and P is that of the target nucleon. W is the invariant mass of the unobserved hadronic final state.

Fig. 7 Separation of the structure functions with data at constant ν and q^2 but different angles. The solid lines are straight line fits to $\sigma_T + \epsilon \sigma_S$ at $q^2 = 4(\text{GeV}/c)^2$ and W = 2, 3, and 4 GeV. $R \equiv \sigma_S / \sigma_T$.

Fig. 8 q^2- ν plane showing lines on which data have been taken. The shaded area indicates the kinematic region in which interpolated data exist for three or more angles.

Fig. 9 $\sigma_T(q^2, W)$ for W = 2 and 3 GeV as a function of q^2 for the points listed in Table III. The solid line shows $\sigma_{\gamma p}/(1 + q^2/M_\rho^2)^2$ where $\sigma_{\gamma p}$ is the measured total photoabsorption cross section and M_ρ is the mass of the rho meson.

Fig. 10 νW_2 and $2MW_1$ versus $\omega = 2M\nu/q^2$ for the points listed in Table III.

Fig. 11 $2MW_1$ versus ω for $W > 2$ GeV and $q^2 > 1(\text{GeV}/c)^2$ assuming R = 0.18. The ranges of q^2 are given in $(\text{GeV}/c)^2$. Data from each angle are shown.

Fig. 12 νW_2 versus ω for $W > 2$ GeV and $q^2 > 1(\text{GeV}/c)^2$ assuming R = 0.18. The ranges of q^2 are given in $(\text{GeV}/c)^2$. Data from each angle are shown.

Fig. 13 νW_2 versus q^2 for $\omega = 4$ and $W > 2$ GeV.

Fig. 14 νW_2 versus q^2 for $\omega = 1.66$ and for $W > 2$ GeV. The solid line is a fit using a polynomial in $(1 - 1/\omega')$ to all data with $W > 1.8$ GeV and $q^2 > 1(\text{GeV}/c)^2$. $\omega' = \omega + M^2/q^2$.

Fig. 15 νW_2 versus ω' for $W > 2$ GeV and $q^2 > 1 (GeV/c)^2$ assuming $R = 0.18$. The ranges in q^2 are given in $(GeV/c)^2$. Data from all angles are shown.

Fig. 16 νW_2 versus ω for large ω for four ranges of q^2. Preliminary 1970 data. The line at $\nu W_2 = 0.30$ is drawn to facilitate comparisons between the graphs. R is assumed constant and equal to 0.18.

Fig. 17 Values of νW_2 for various ranges of ω plotted against q^2. νW_2 is kinematically constrained to zero for $q^2 = 0$. Preliminary 1970 data. Possible systematic errors are not included in the errors shown. R is assumed constant and equal to 0.18.

Fig. 18 Average values of νW_2 for $q^2 > 1$, for the ranges of ω in Fig. 17. Systematic errors are not shown. R is assumed to be 0.18.

Fig. 19 Ratio of deuterium to hydrogen cross sections for various values of W as a function of q^2. These are preliminary results including rough radiative corrections. The points at $q^2 = 0$ are taken from total photoabsorption cross section measurements.

Fig. 20 The quantity (D/H - 1) plotted against ω. The data are preliminary. If corrections for internal motion of the nucleons in deuterium, final state interactions and Glauber corrections are small, the ordinate should approximate the ratio of neutron to proton scattering cross sections.

Fig. 21(a) The upper graph shows $(\nu W_{2p} - \nu W_{2n})$ derived from the points in Fig. 20 and from the fit to νW_{2p} discussed in the text. There is the suggestion of a maximum around $\omega \sim 3$.

(b) The lower graph shows νW_2 versus ω as originally estimated from general considerations[15], and as calculated from simple phase space considerations[12]. These νW_2 curves have shapes qualitatively similar to the points for $\Delta (\nu W_2)$ in (a).

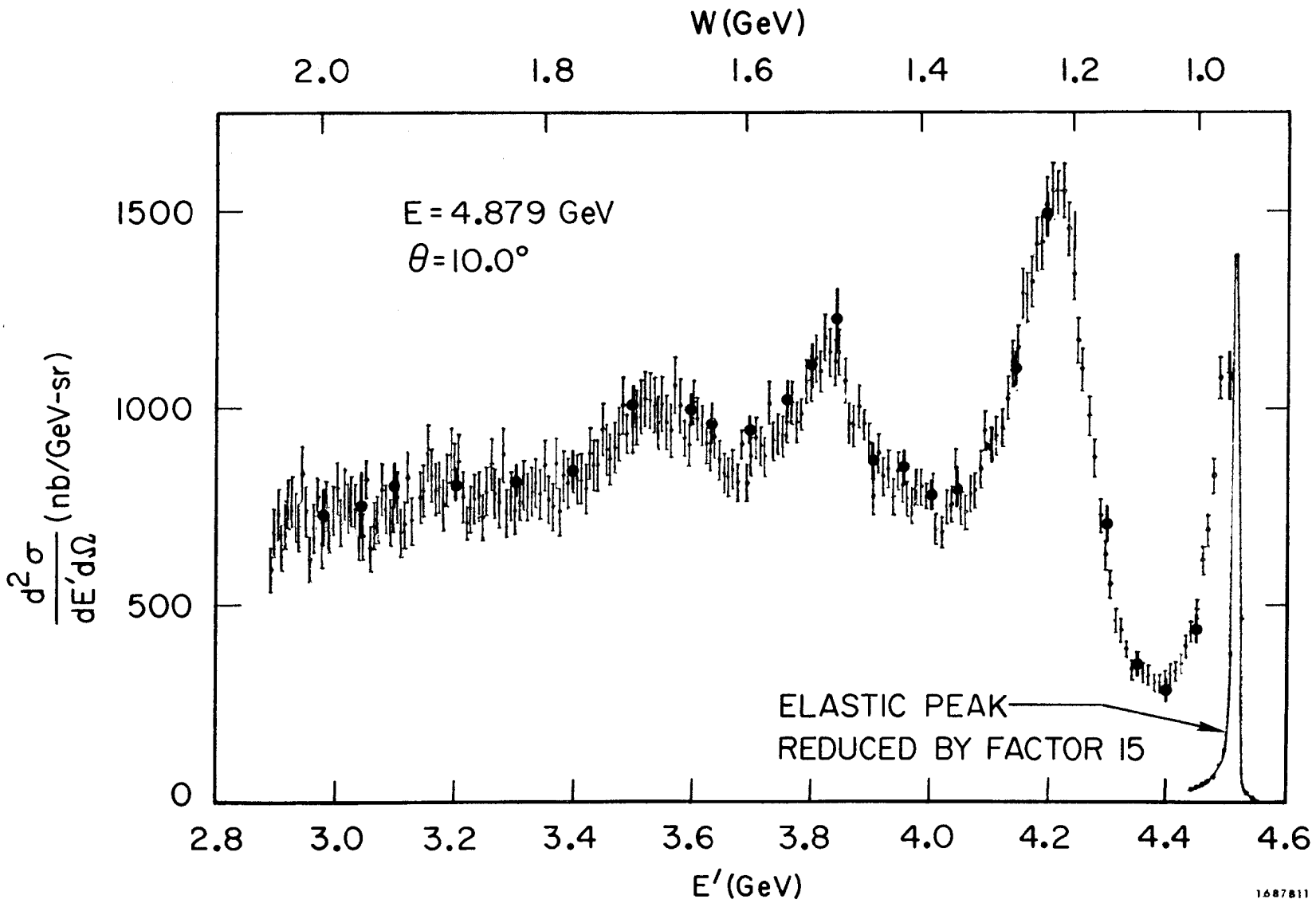
W(GeV)
2.0
1.8
1.6
1.4
1.2
1.0
E = 4.879 GeV
θ = 10.0°
1500
1000
500
0
$\frac{d^2\sigma}{dE'd\Omega}$ (nb/GeV-sr)
ELASTIC PEAK
REDUCED BY FACTOR 15
2.8
3.0
3.2
3.4
3.6
3.8
4.0
4.2
4.4
4.6
E′(GeV)
1687811

FIG 1

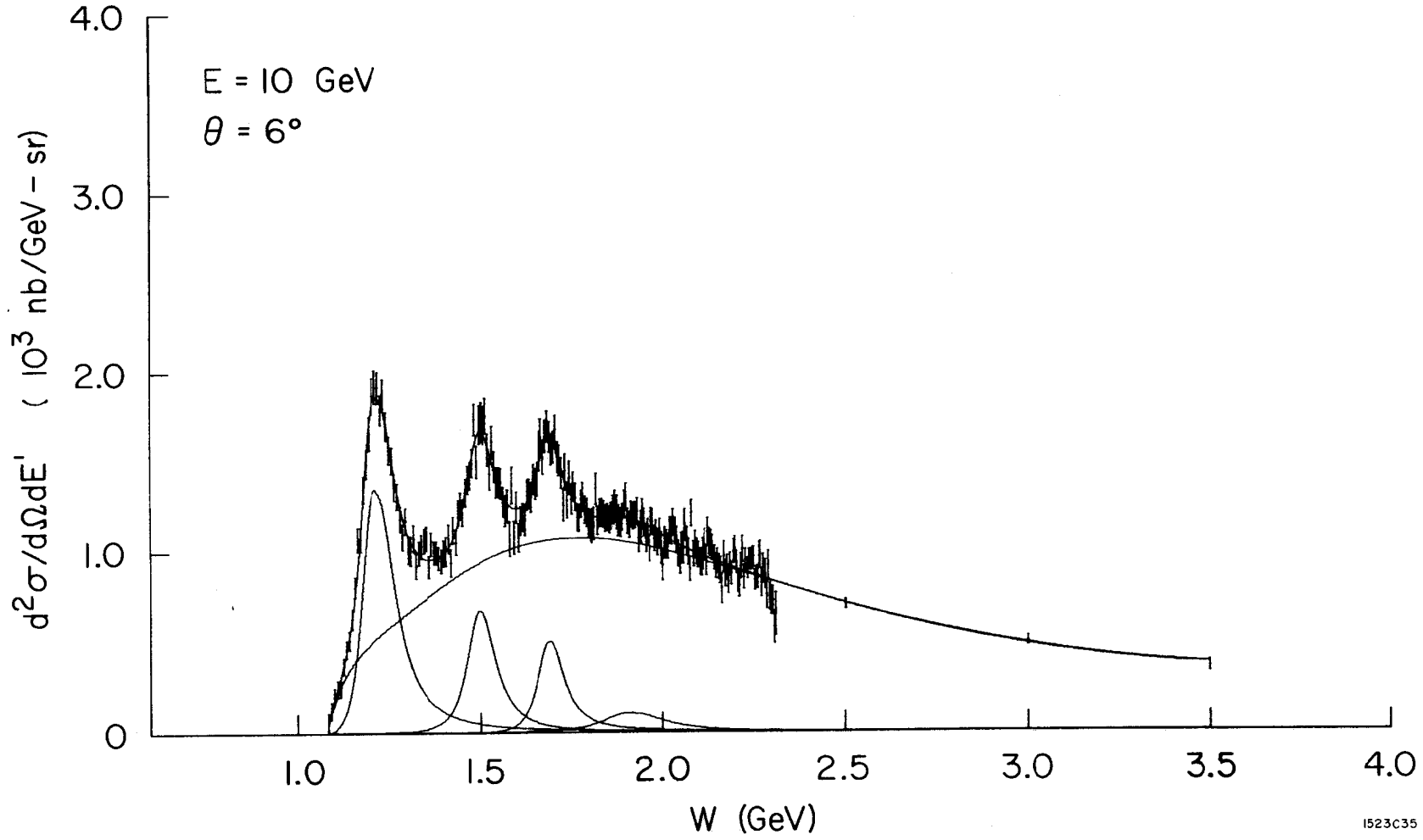
E = 10 GeV
θ = 6°
$d^2\sigma/d\Omega dE'$ (10^3 nb/GeV – sr)
4.0
3.0
2.0
1.0
0
1.0
1.5
2.0
2.5
3.0
3.5
4.0
W (GeV)
1523C35

FIG 2

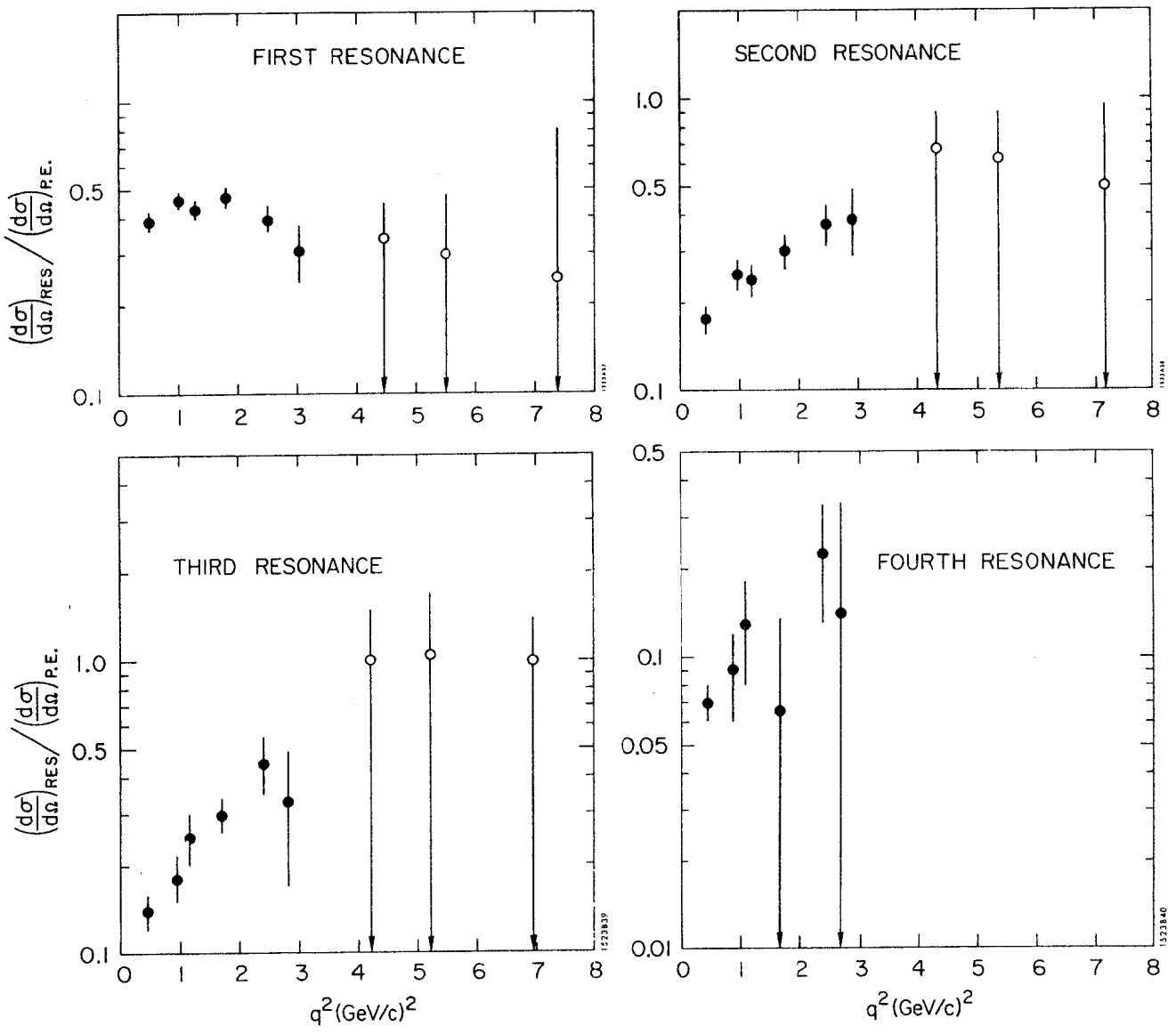
FIRST RESONANCE
SECOND RESONANCE
THIRD RESONANCE
FOURTH RESONANCE
$\left(\frac{d\sigma}{d\Omega}\right)_{RES} / \left(\frac{d\sigma}{d\Omega}\right)_{P.E.}$
q^2(GeV/c)^2

FIG 3

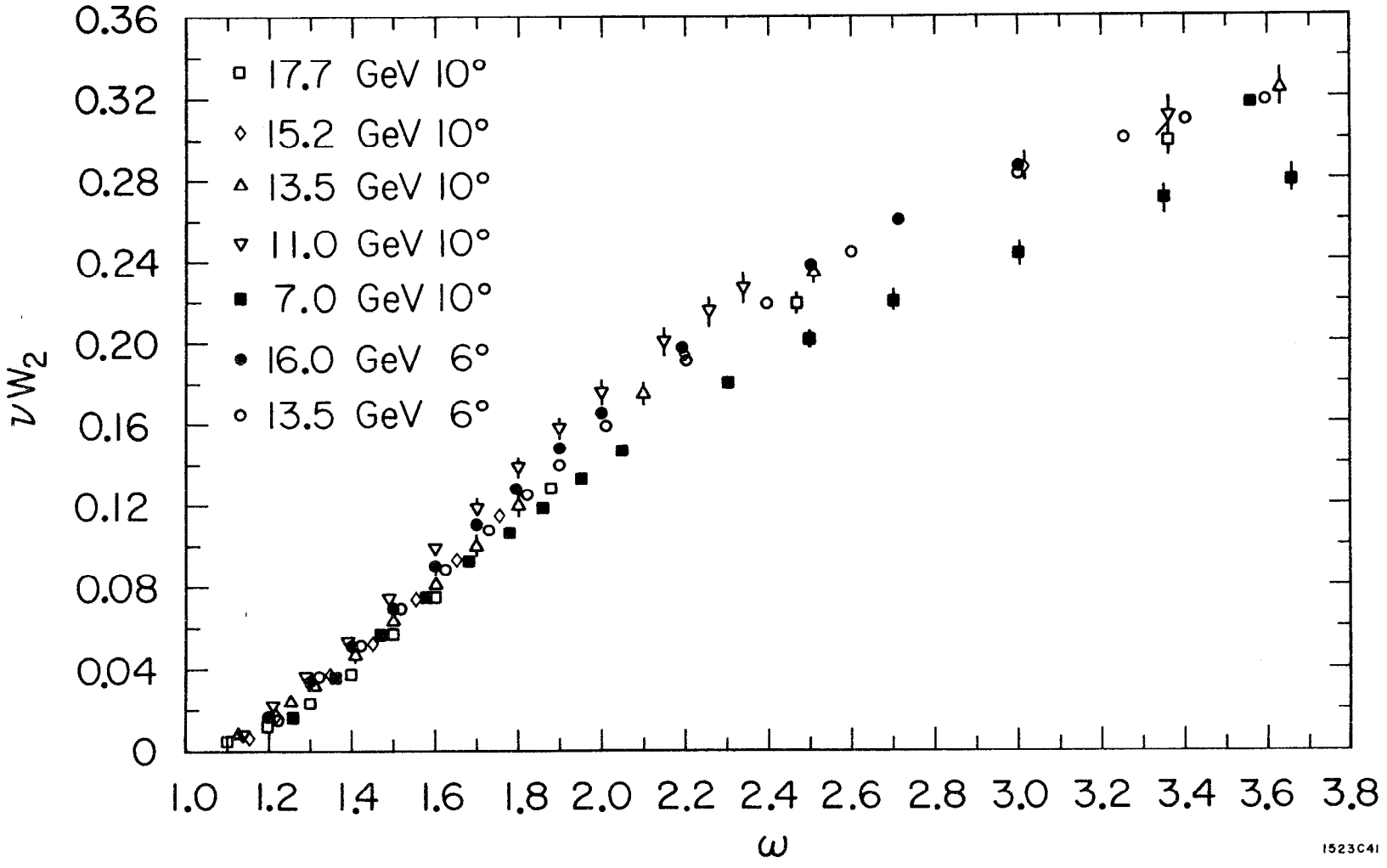
0.36
0.32
0.28
0.24
0.20
0.16
0.12
0.08
0.04
0
νW_2
17.7 GeV 10°
15.2 GeV 10°
13.5 GeV 10°
11.0 GeV 10°
7.0 GeV 10°
16.0 GeV 6°
13.5 GeV 6°
1.0 1.2 1.4 1.6 1.8 2.0 2.2 2.4 2.6 2.8 3.0 3.2 3.4 3.6 3.8
ω
1523C41

FIG 4

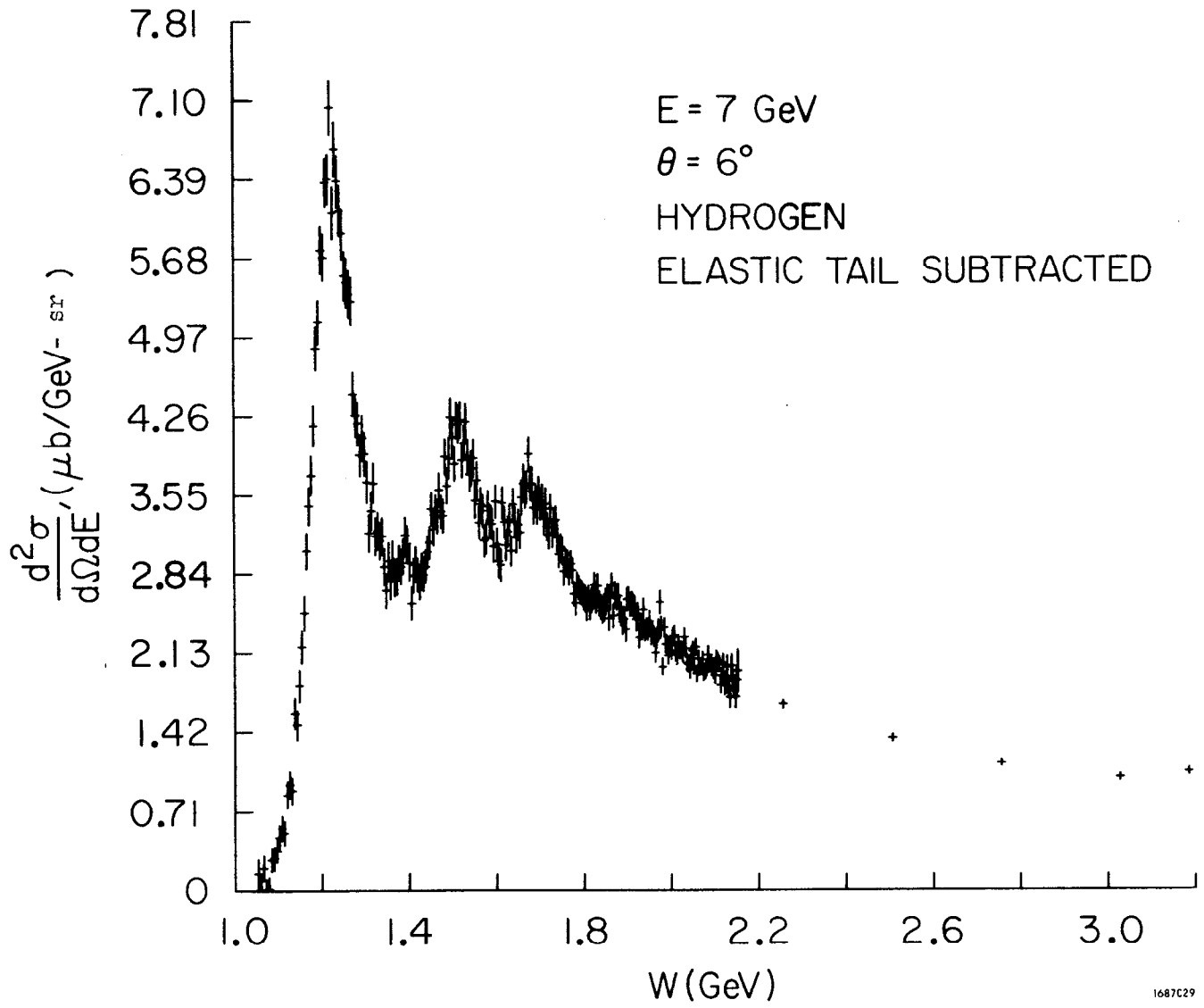
7.81
7.10
6.39
5.68
4.97
4.26
3.55
2.84
2.13
1.42
0.71
0
$\frac{d^2\sigma}{d\Omega dE'}$ (μb/GeV-sr)
E = 7 GeV
θ = 6°
HYDROGEN
ELASTIC TAIL SUBTRACTED
1.0
1.4
1.8
2.2
2.6
3.0
W(GeV)
1687C29

FIG 5a

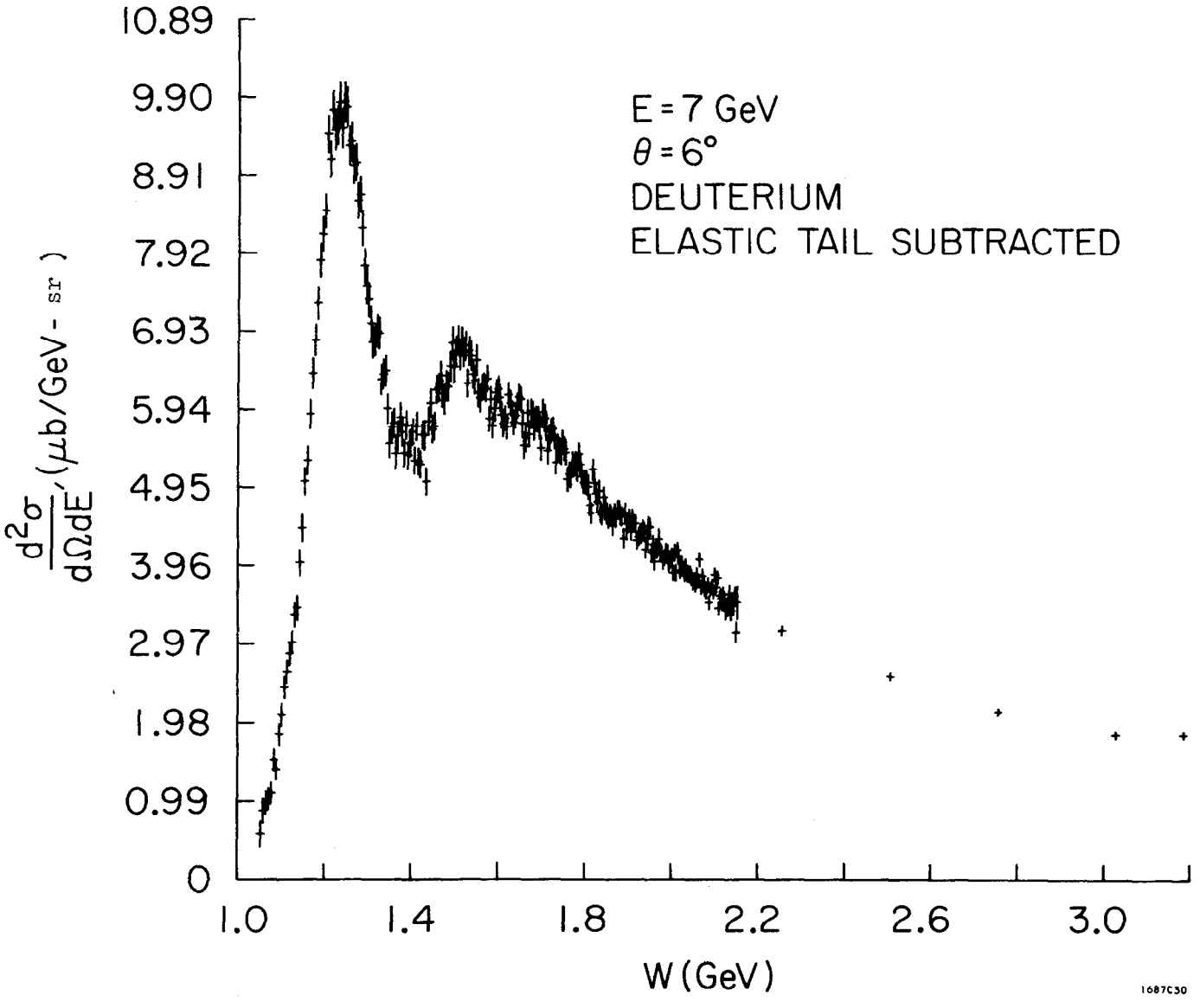
10.89
9.90
8.91
7.92
6.93
5.94
4.95
3.96
2.97
1.98
0.99
0
1.0
1.4
1.8
2.2
2.6
3.0
W (GeV)
$\frac{d^2\sigma}{d\Omega dE'}$ (μb/GeV - sr)
E = 7 GeV
θ = 6°
DEUTERIUM
ELASTIC TAIL SUBTRACTED
1687C30

FIG 5b

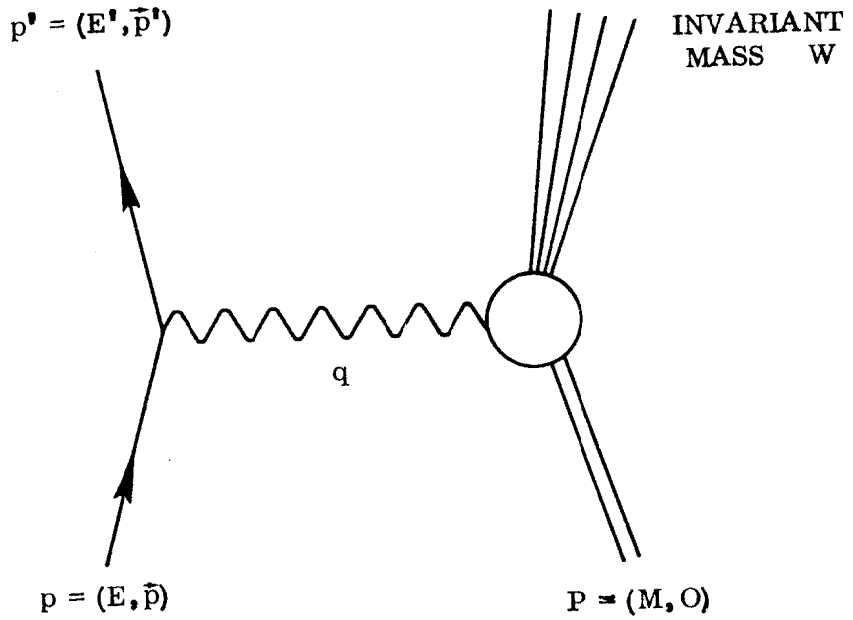

FIG 6

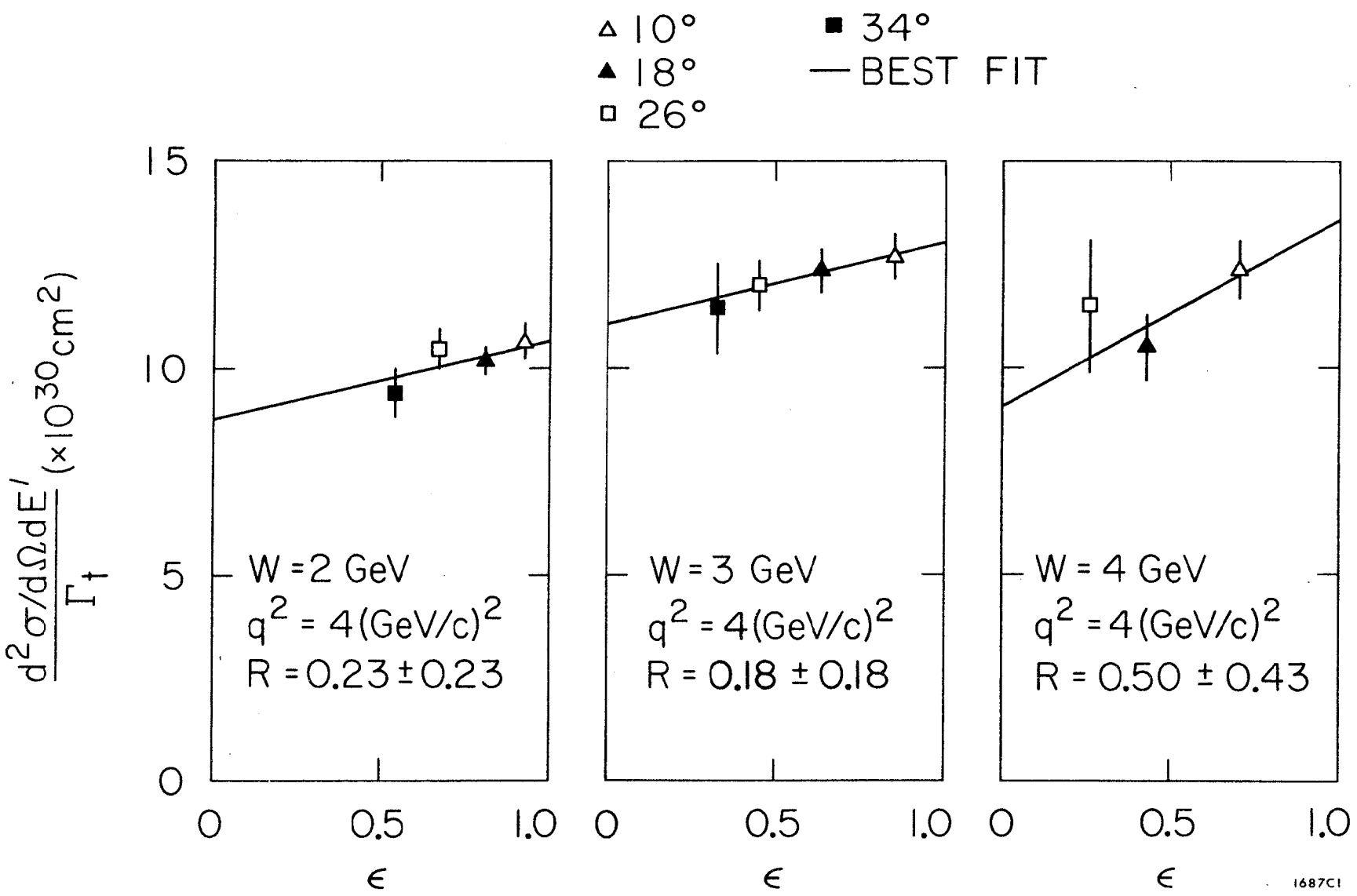
△ 10°
▲ 18°
□ 26°
■ 34°
— BEST FIT
$\frac{d^2\sigma/d\Omega dE'}{\Gamma_t}$ (×10^{30}cm^2)
15
10
5
0
W = 2 GeV
q^2 = 4(GeV/c)^2
R = 0.23 ± 0.23
W = 3 GeV
q^2 = 4(GeV/c)^2
R = 0.18 ± 0.18
W = 4 GeV
q^2 = 4(GeV/c)^2
R = 0.50 ± 0.43
0
0.5
1.0
ε
1687C1

FIG 7

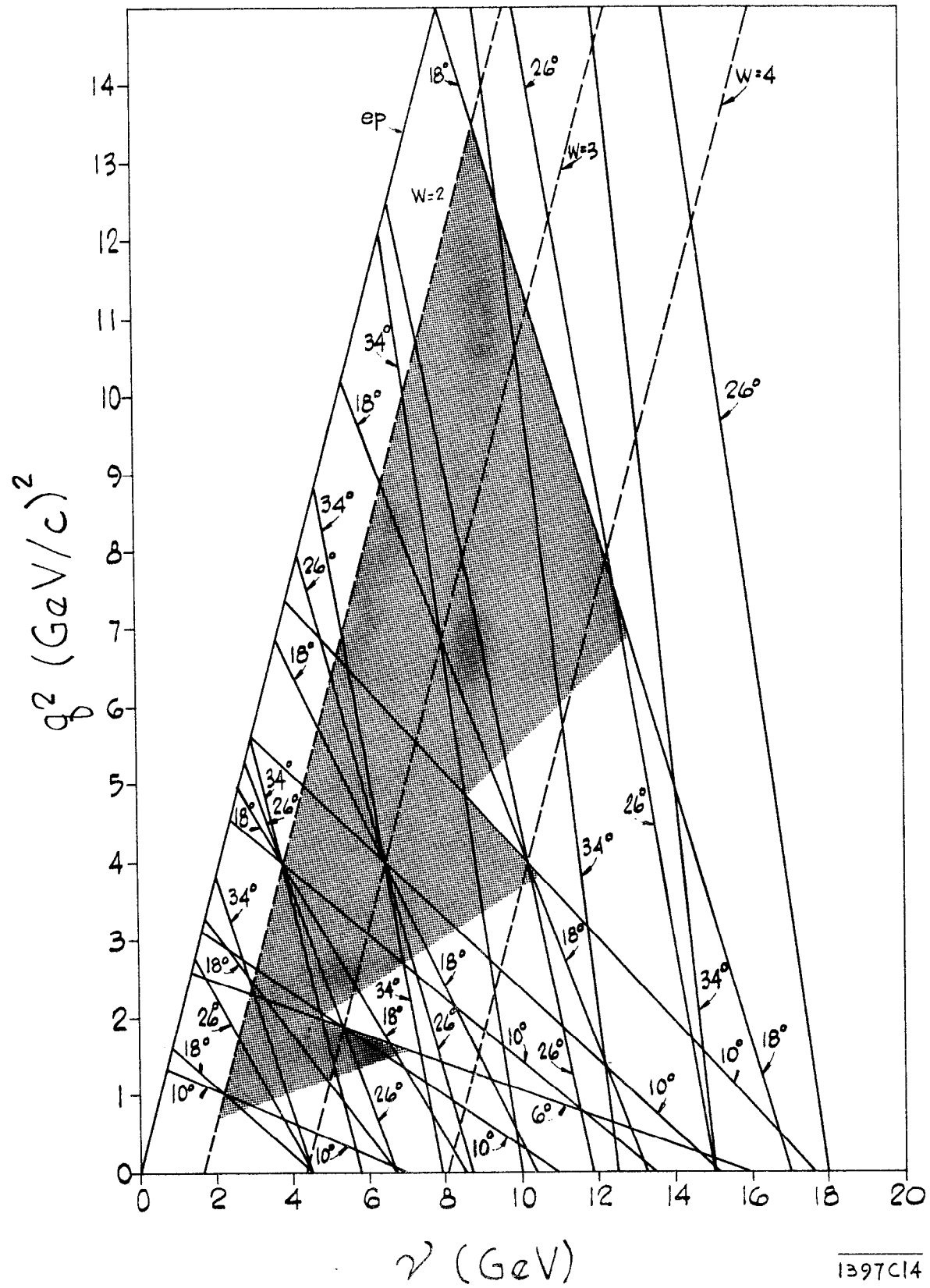
ep
W=2
W=3
W=4
18°
26°
34°
10°
6°
q^2 (GeV/c)^2
ν (GeV)
0
2
4
6
8
10
12
14
16
18
20
1397C14

FIG 8

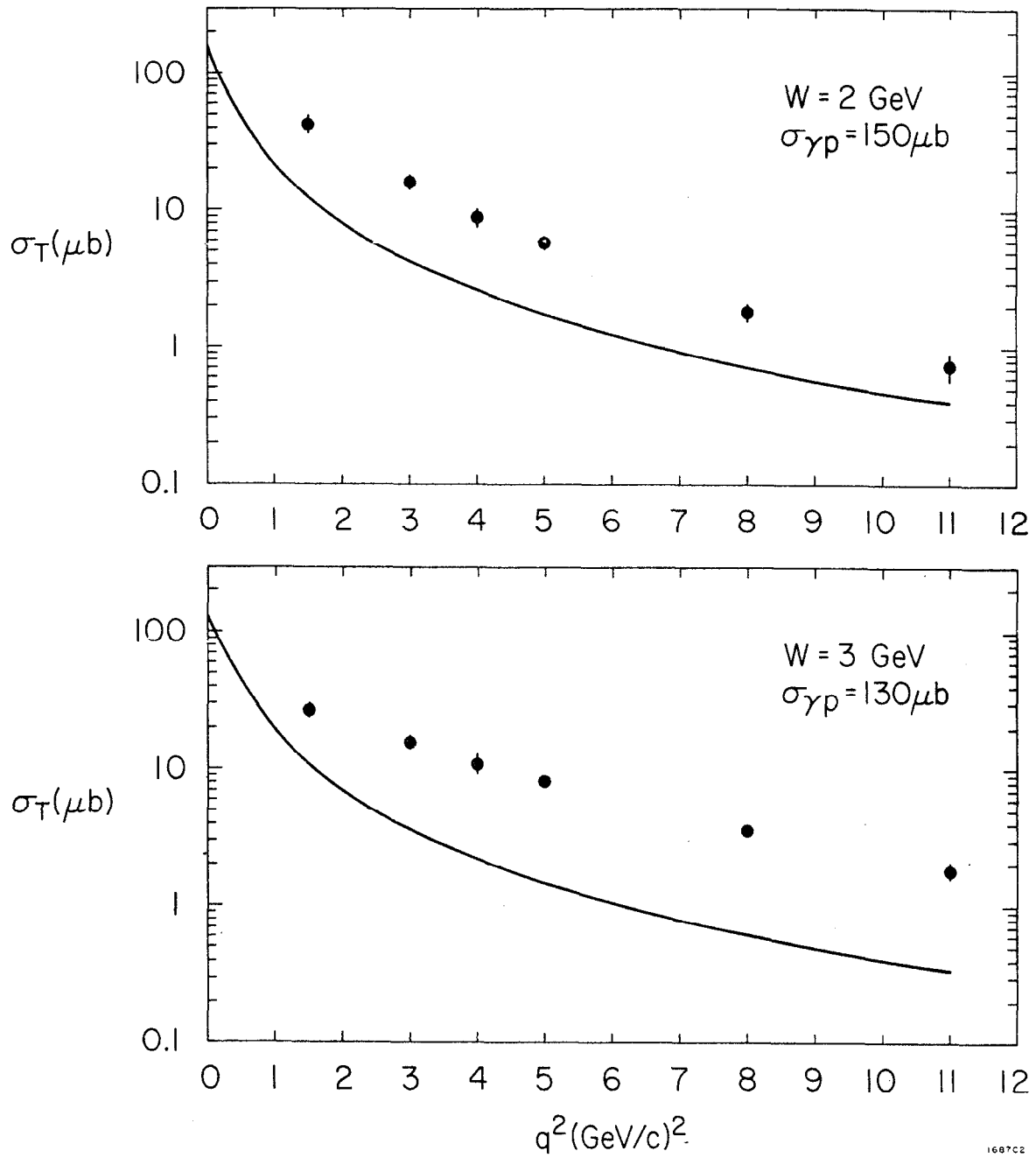
W = 2 GeV
$\sigma_{\gamma p}$ = 150μb
W = 3 GeV
$\sigma_{\gamma p}$ = 130μb
$\sigma_T(\mu b)$
100
10
1
0.1
0 1 2 3 4 5 6 7 8 9 10 11 12
q^2(GeV/c)^2
1687C2

FIG 9

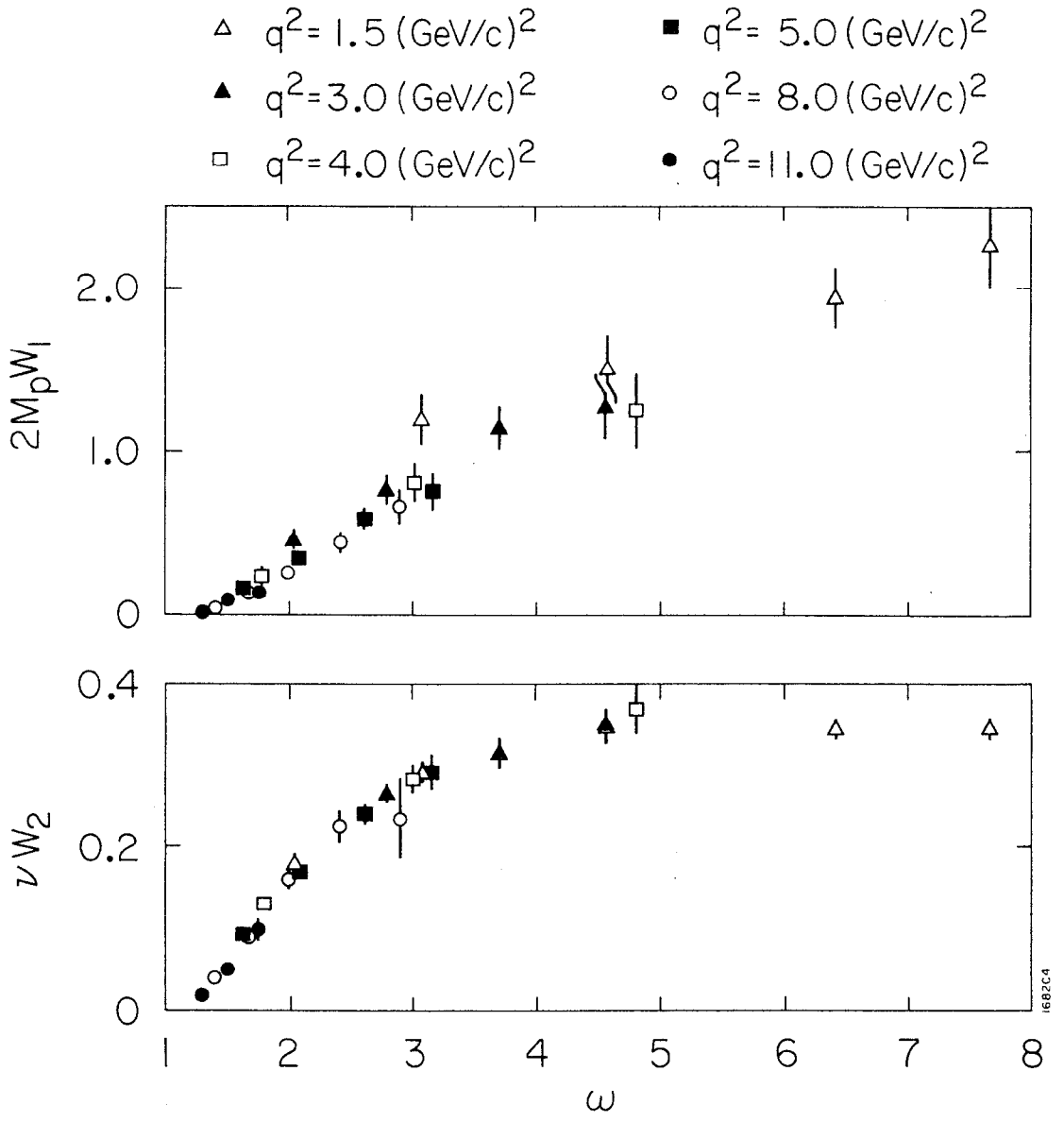
q^2= 1.5 (GeV/c)^2
q^2= 5.0 (GeV/c)^2
q^2=3.0 (GeV/c)^2
q^2= 8.0 (GeV/c)^2
q^2=4.0 (GeV/c)^2
q^2=11.0 (GeV/c)^2
$2M_pW_1$
νW_2
ω
0
1.0
2.0
0.2
0.4
1
2
3
4
5
6
7
8
1682C4

FIG 10

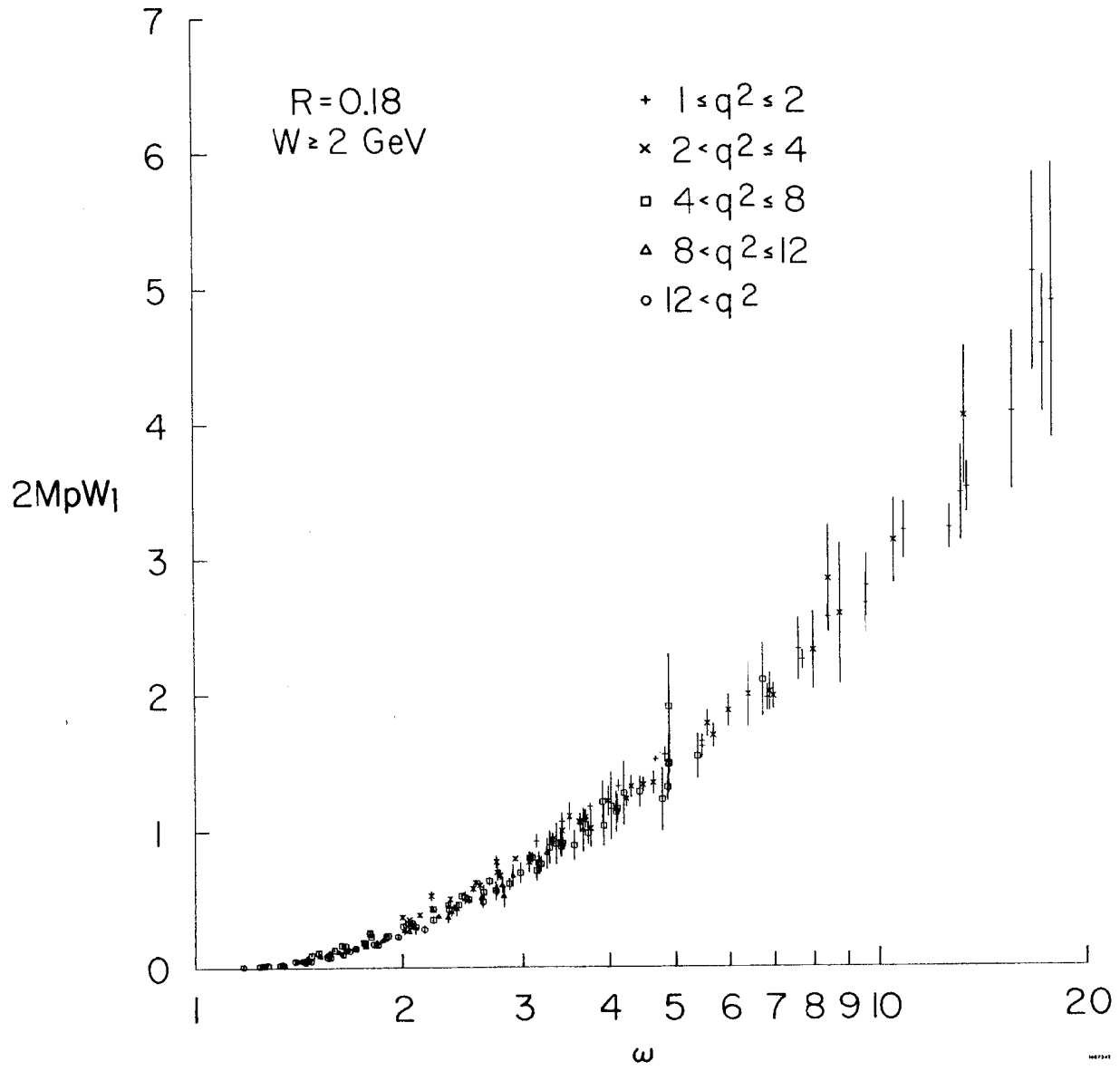
R=0.18
W≥2 GeV
+ 1≤q²≤2
× 2<q²≤4
□ 4<q²≤8
△ 8<q²≤12
○ 12<q²
2MpW1
0
1
2
3
4
5
6
7
1
2
3
4
5
6
7
8
9
10
20
ω

FIG 11

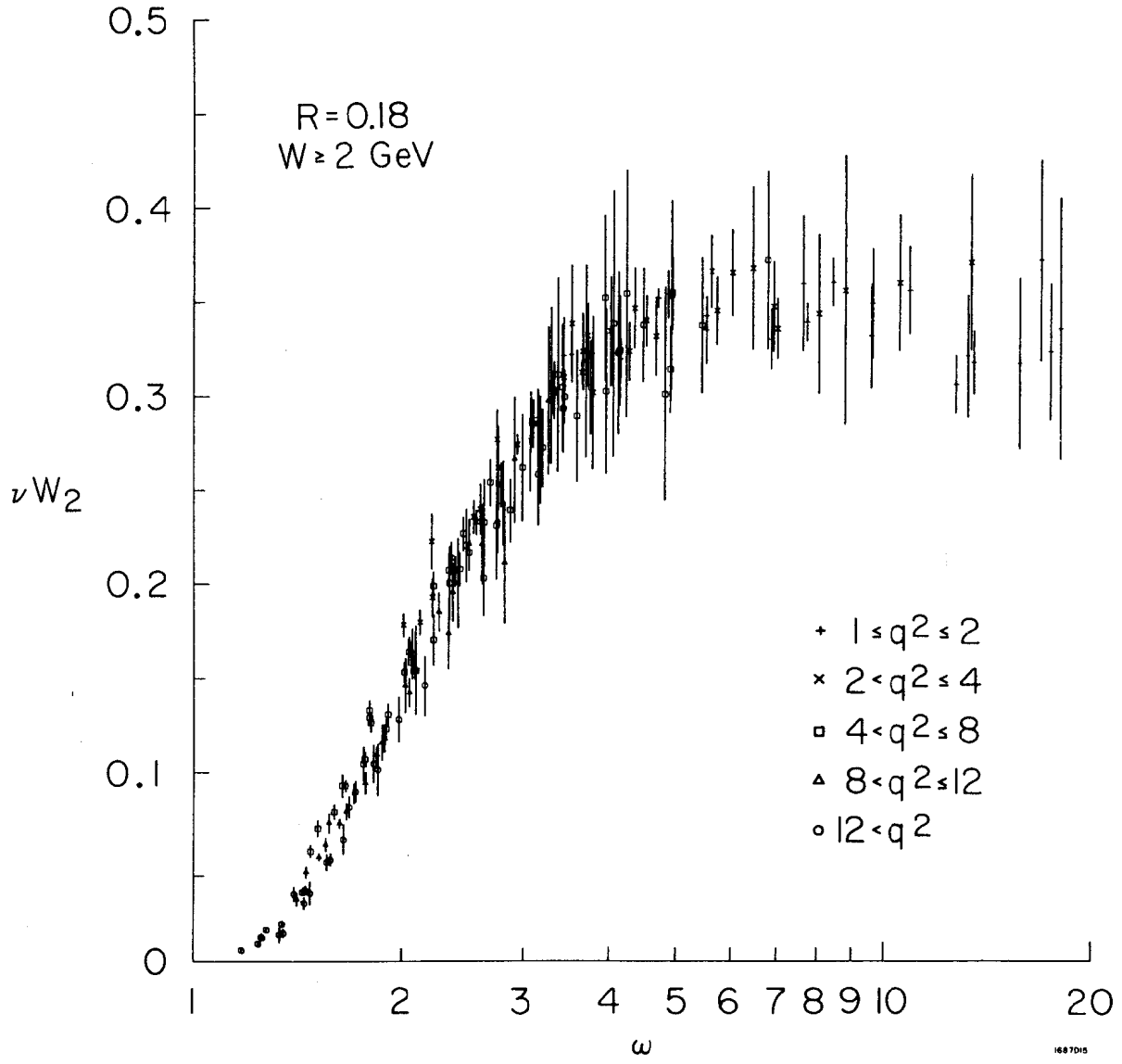
0.5
0.4
0.3
0.2
0.1
0
νW2
R=0.18
W≥2 GeV
+ 1≤q2≤2
× 2<q2≤4
□ 4<q2≤8
△ 8<q2≤12
○ 12<q2
1
2
3
4
5
6
7
8
9
10
20
ω

FIG 12

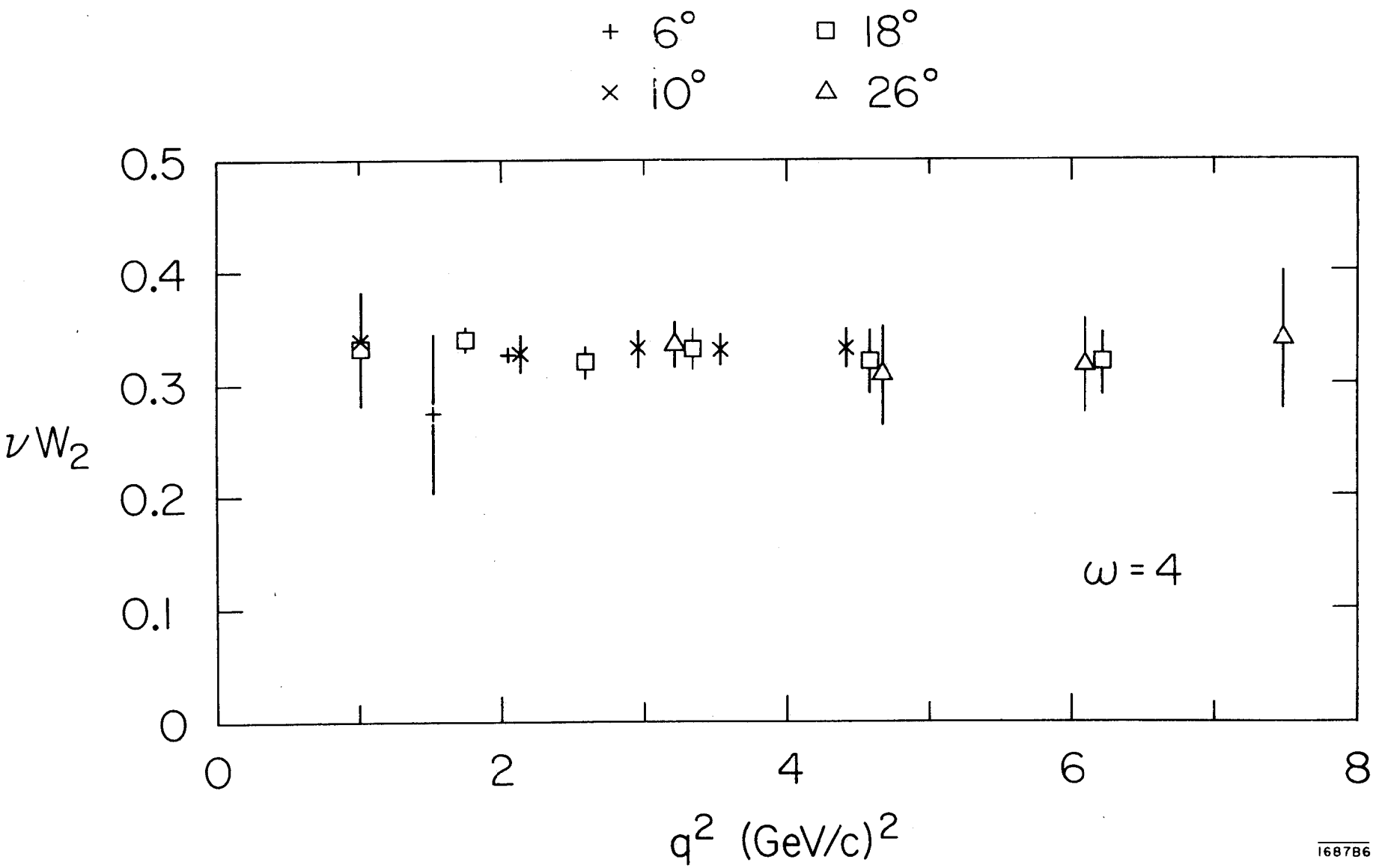

FIG 13

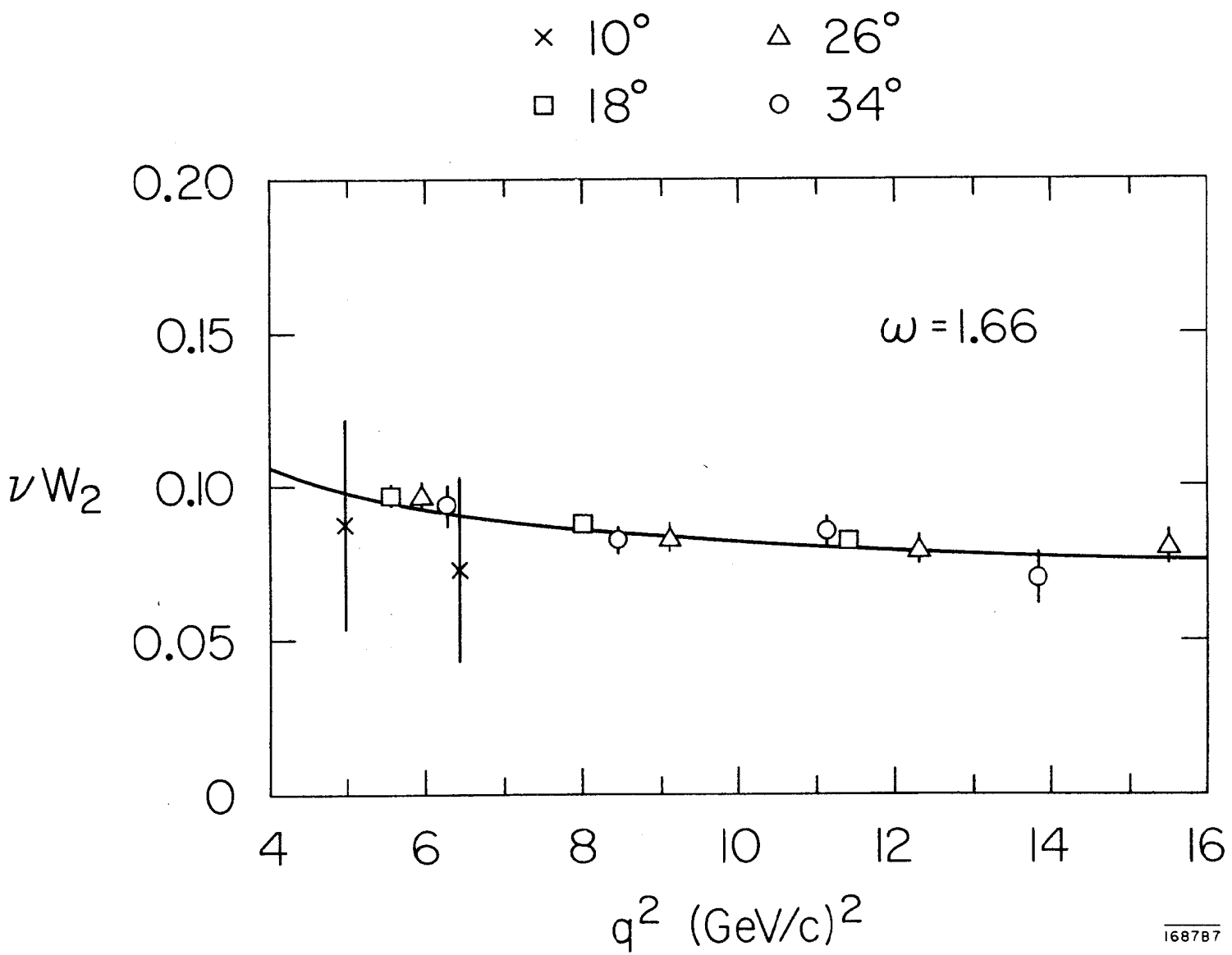
× 10°
△ 26°
□ 18°
○ 34°
0.20
0.15
0.10
0.05
0
νW_2
ω = 1.66
4
6
8
10
12
14
16
q^2 (GeV/c)^2
168787

FIG 14

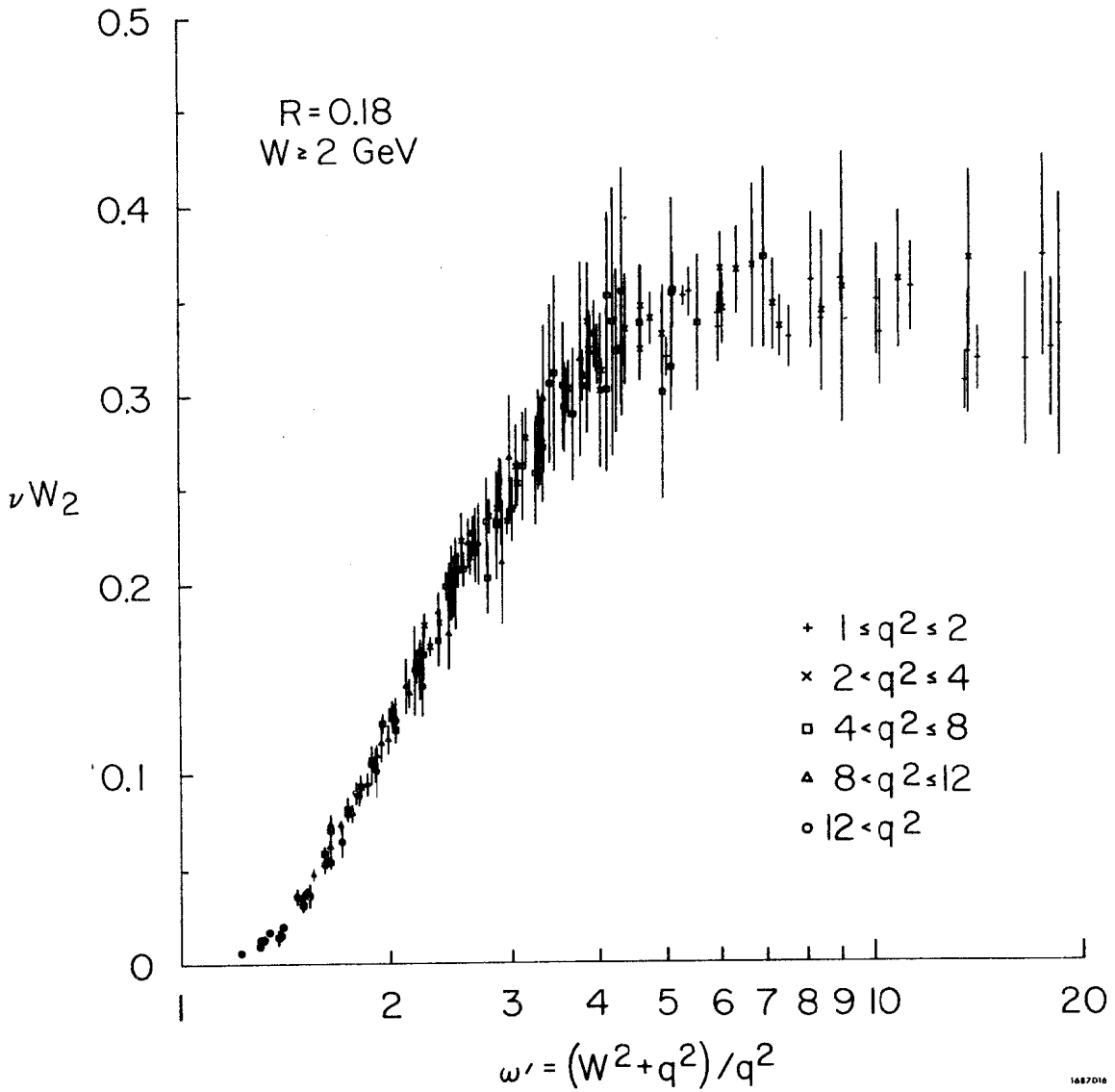
0.5
0.4
0.3
0.2
0.1
0
νW_2
R = 0.18
W ≥ 2 GeV
+ $1 \le q^2 \le 2$
× $2 < q^2 \le 4$
□ $4 < q^2 \le 8$
△ $8 < q^2 \le 12$
○ $12 < q^2$
1
2
3
4
5
6
7
8
9
10
20
$\omega' = (W^2+q^2)/q^2$
1687016

FIG 15

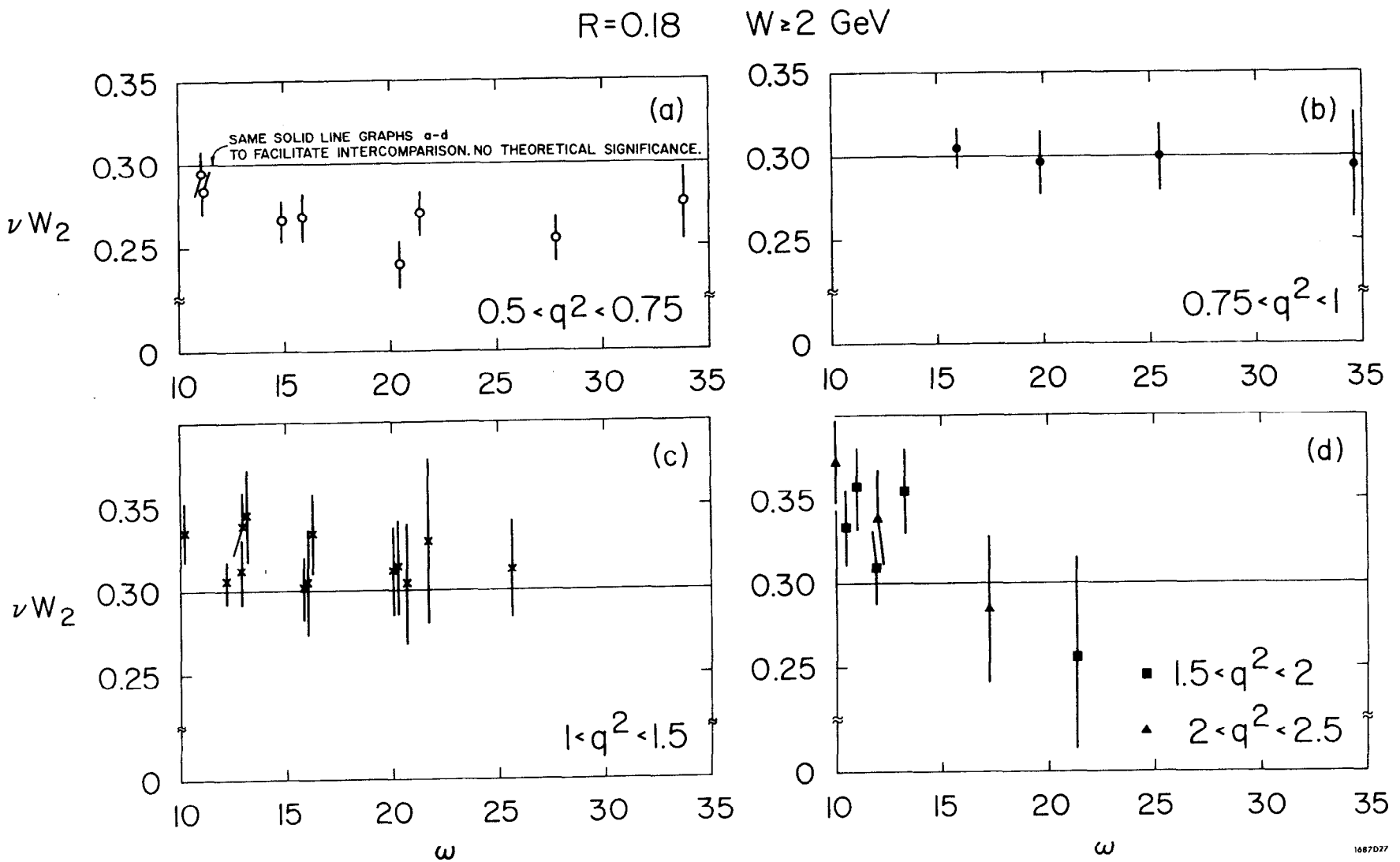
R=0.18
W≥2 GeV
(a)
SAME SOLID LINE GRAPHS a-d
TO FACILITATE INTERCOMPARISON. NO THEORETICAL SIGNIFICANCE.
0.5<q2<0.75
(b)
0.75<q2<1
(c)
1<q2<1.5
(d)
1.5<q2<2
2<q2<2.5
νW2
ω
0.35
0.30
0.25
0
10
15
20
25
30
35
1687D27

FIG 16

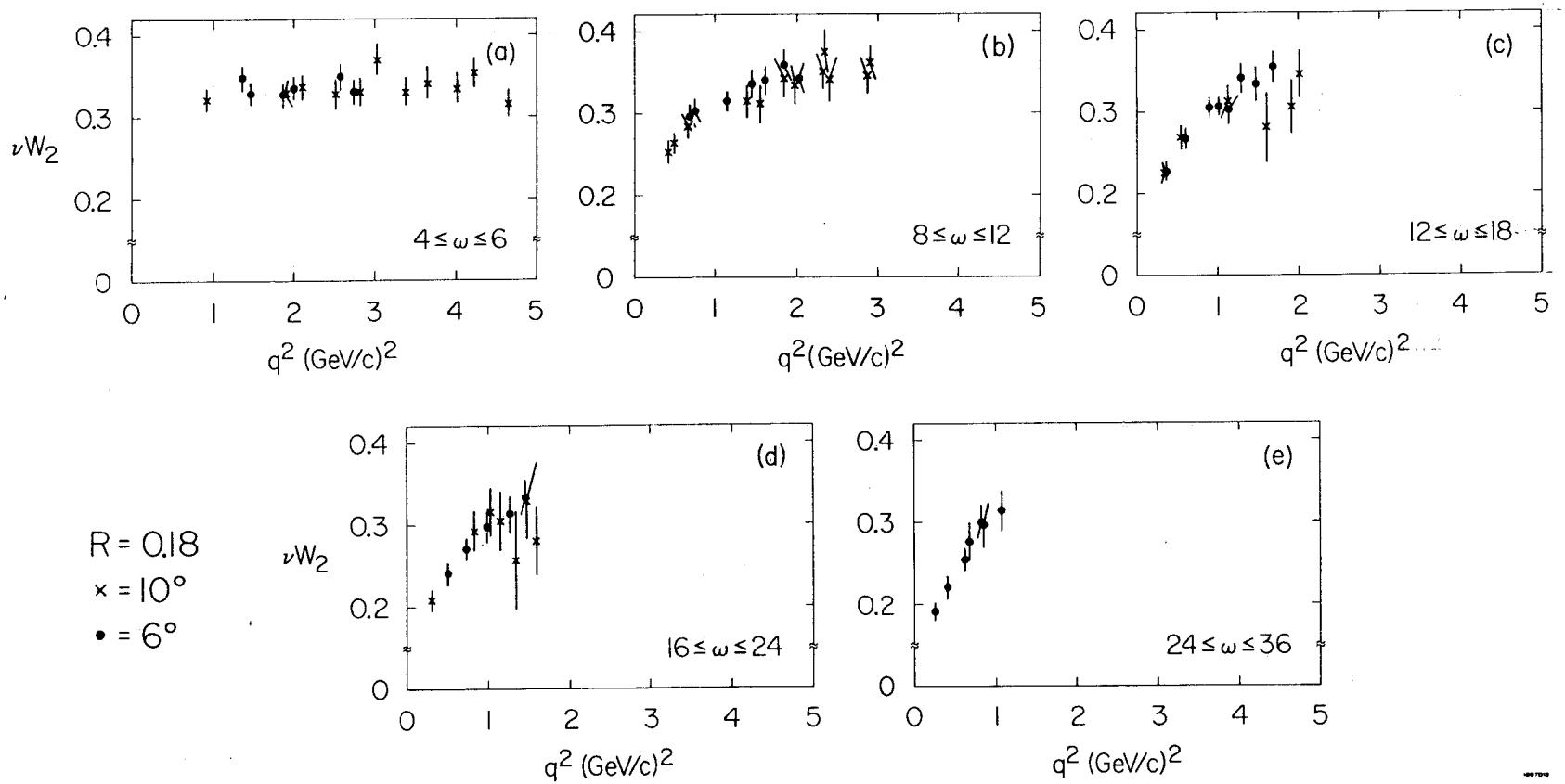
(a)
(b)
(c)
(d)
(e)
νW_2
q^2 (GeV/c)^2
$4 \le \omega \le 6$
$8 \le \omega \le 12$
$12 \le \omega \le 18$
$16 \le \omega \le 24$
$24 \le \omega \le 36$
R = 0.18
× = 10°
• = 6°

FIG 17

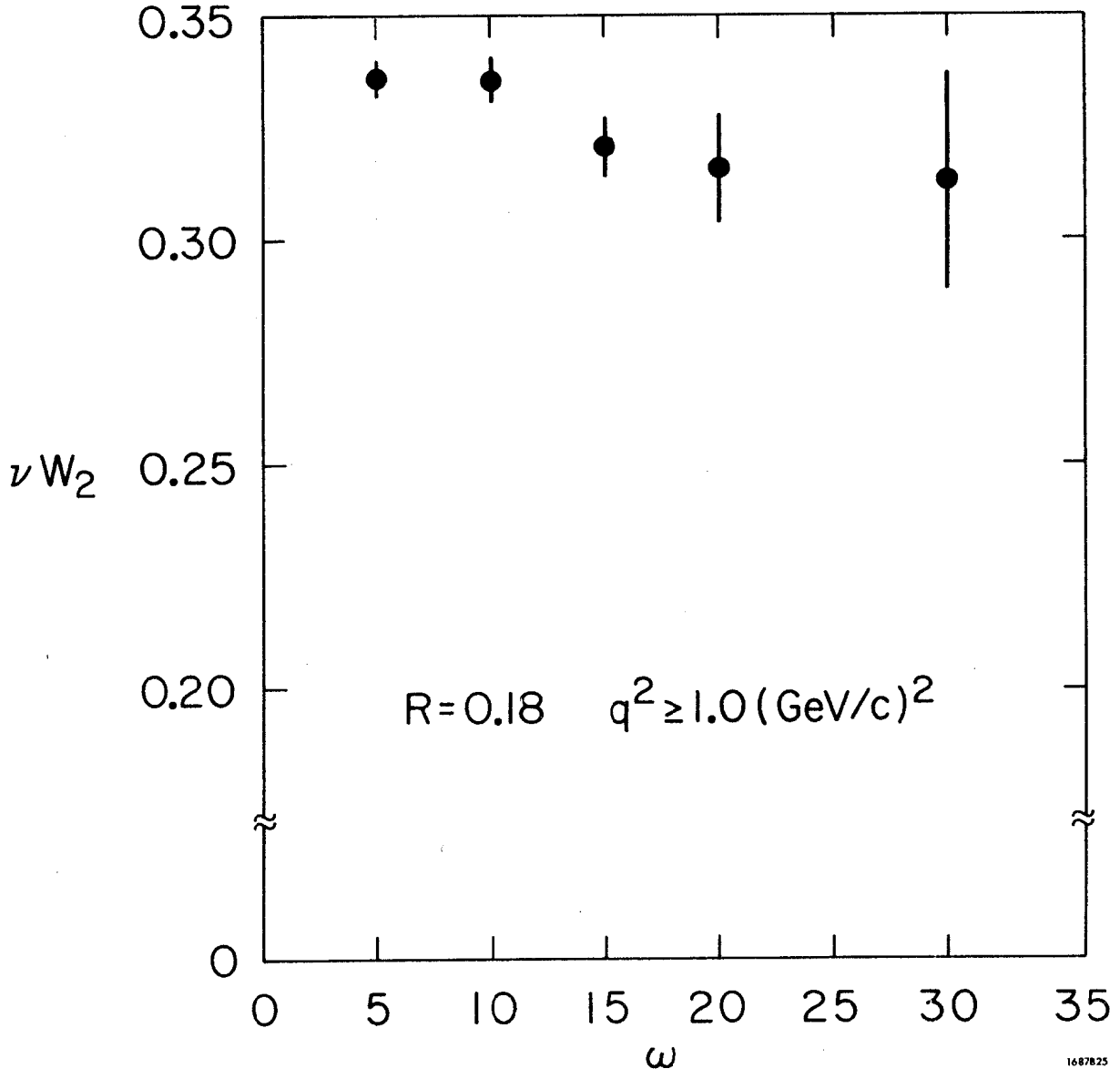
0.35
0.30
0.25
0.20
0
νW_2
R=0.18 $q^2 \geq 1.0$ (GeV/c)^2
0 5 10 15 20 25 30 35
ω
1687B25

FIG 18

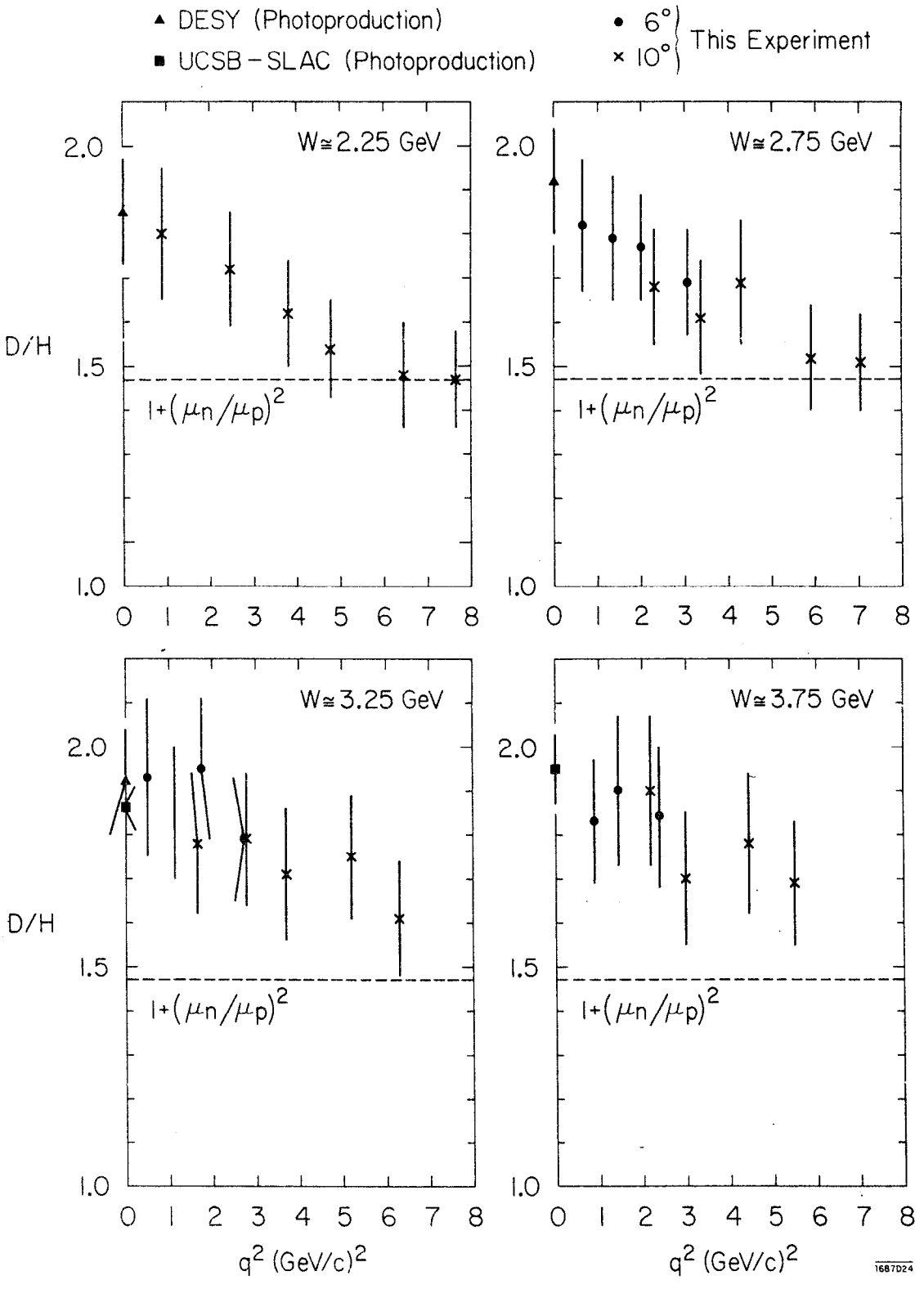
▲ DESY (Photoproduction)
■ UCSB – SLAC (Photoproduction)
• 6°
× 10°
This Experiment
W≅2.25 GeV
W≅2.75 GeV
W≅3.25 GeV
W≅3.75 GeV
D/H
2.0
1.5
1.0
1+(μn/μp)²
0 1 2 3 4 5 6 7 8
q² (GeV/c)²
1687D24

FIG 19

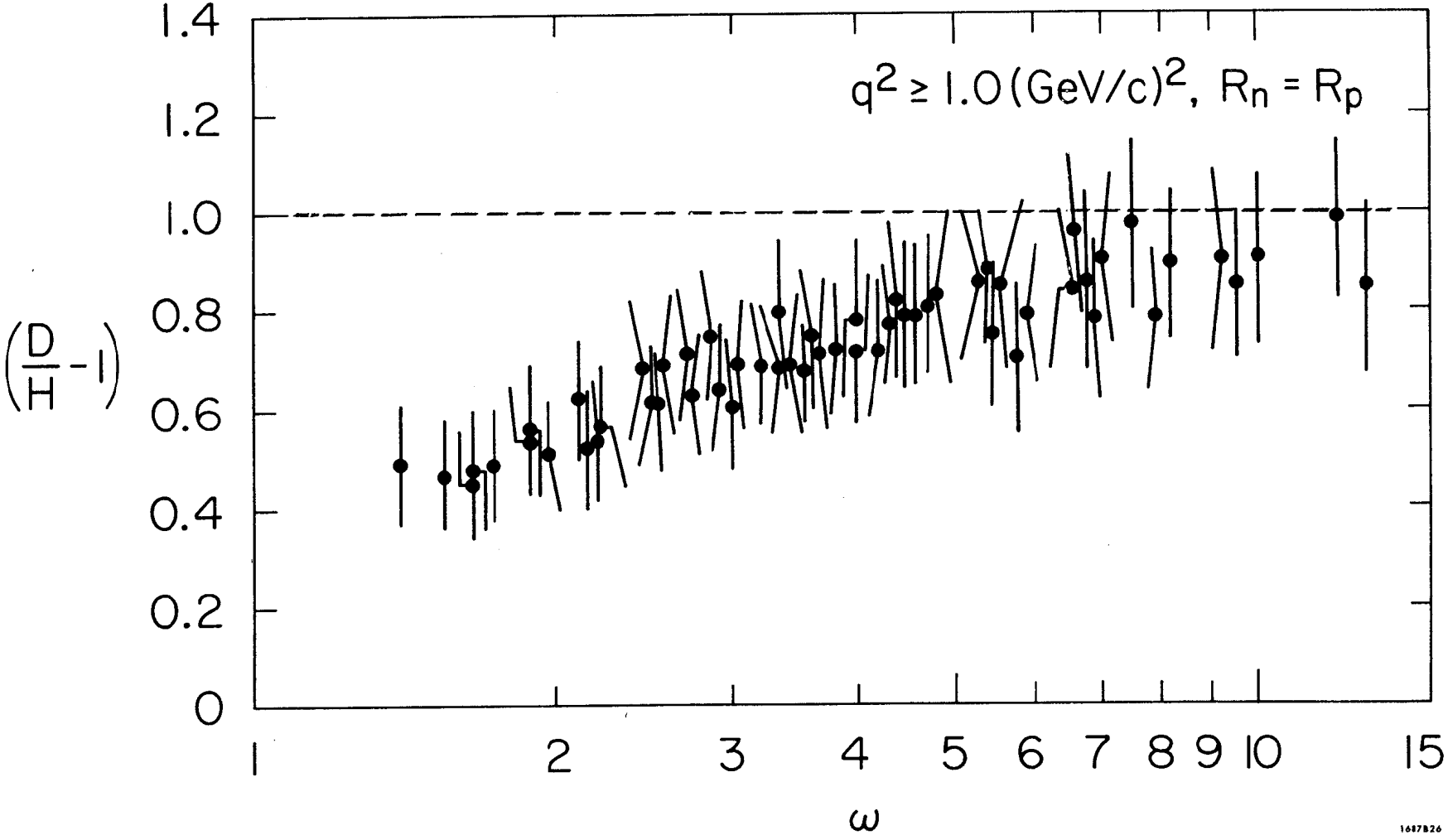
$q^2 \geq 1.0\,(GeV/c)^2$, $R_n = R_p$
$\left(\frac{D}{H} - 1\right)$
1.4
1.2
1.0
0.8
0.6
0.4
0.2
0
1
2
3
4
5
6
7
8
9
10
15
ω
1617B26

FIG 20

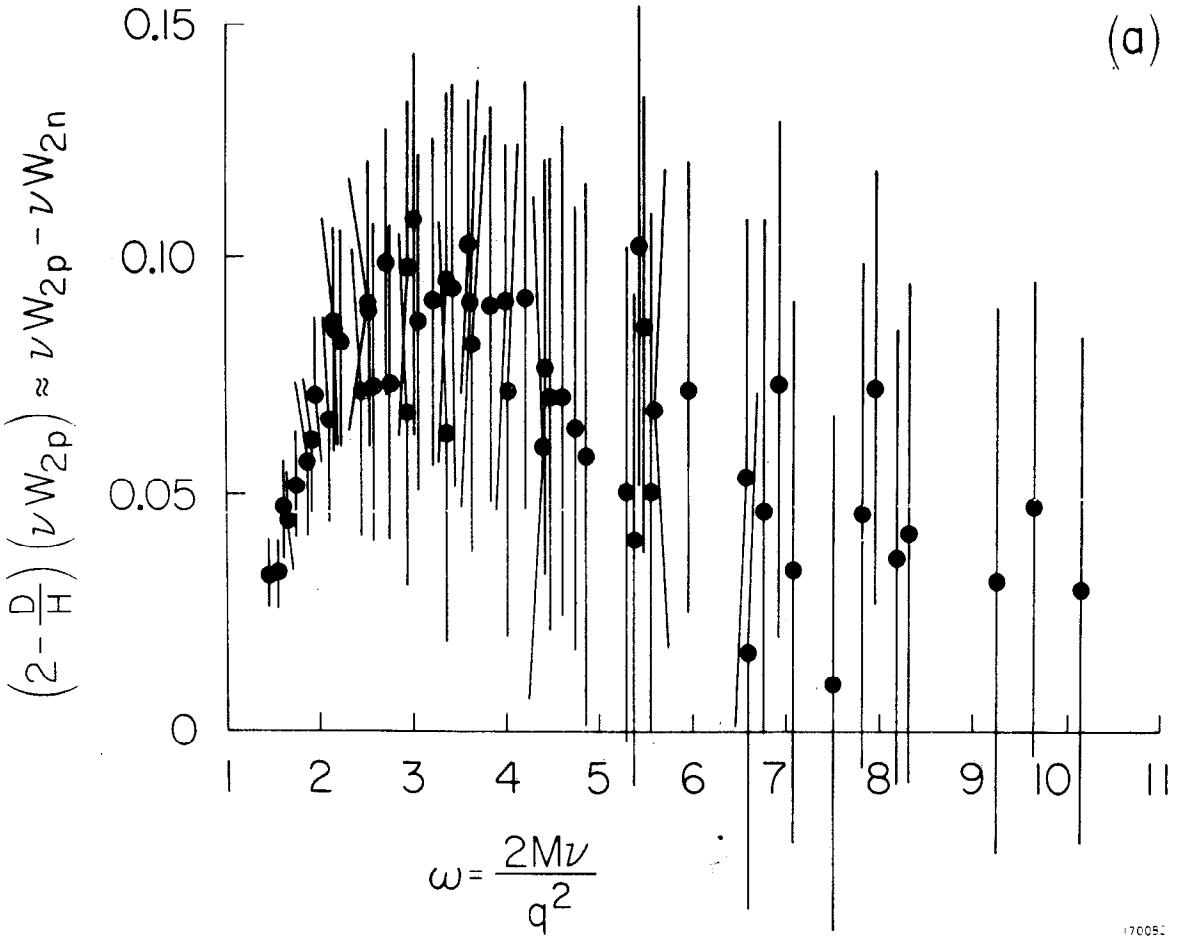
(a)
0.15
0.10
0.05
0
$\left(2-\frac{D}{H}\right)\left(\nu W_{2p}\right) \approx \nu W_{2p} - \nu W_{2n}$
1 2 3 4 5 6 7 8 9 10 11
$\omega = \frac{2M\nu}{q^2}$
170052

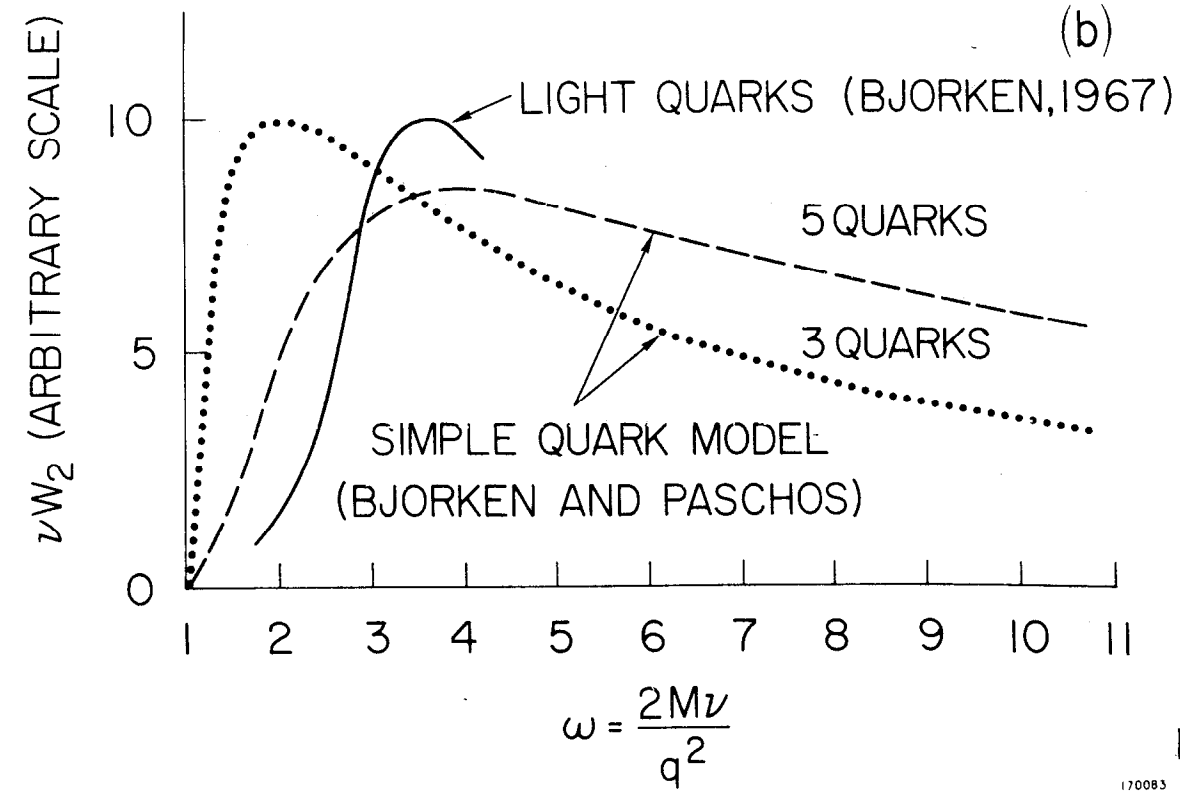
(b)
LIGHT QUARKS (BJORKEN,1967)
5 QUARKS
3 QUARKS
SIMPLE QUARK MODEL
(BJORKEN AND PASCHOS)
νW_2 (ARBITRARY SCALE)
10
5
0
1 2 3 4 5 6 7 8 9 10 11
$\omega = \frac{2M\nu}{q^2}$
170083

Fig. 21